AD-A055 198 AIR FORCE INST OF TECH WRIGHT-PATTERSON AFB OHIO SCH--ETC F/G 20/12
DEEP LEVEL TRAP SPECTROSCOPY OF GALLIUM ARSENIDE.(U)
MAR 78 C E MAYO

UNCLASSIFIED AFIT/GE/EE/78-4 NL

| OF
AD
A055198

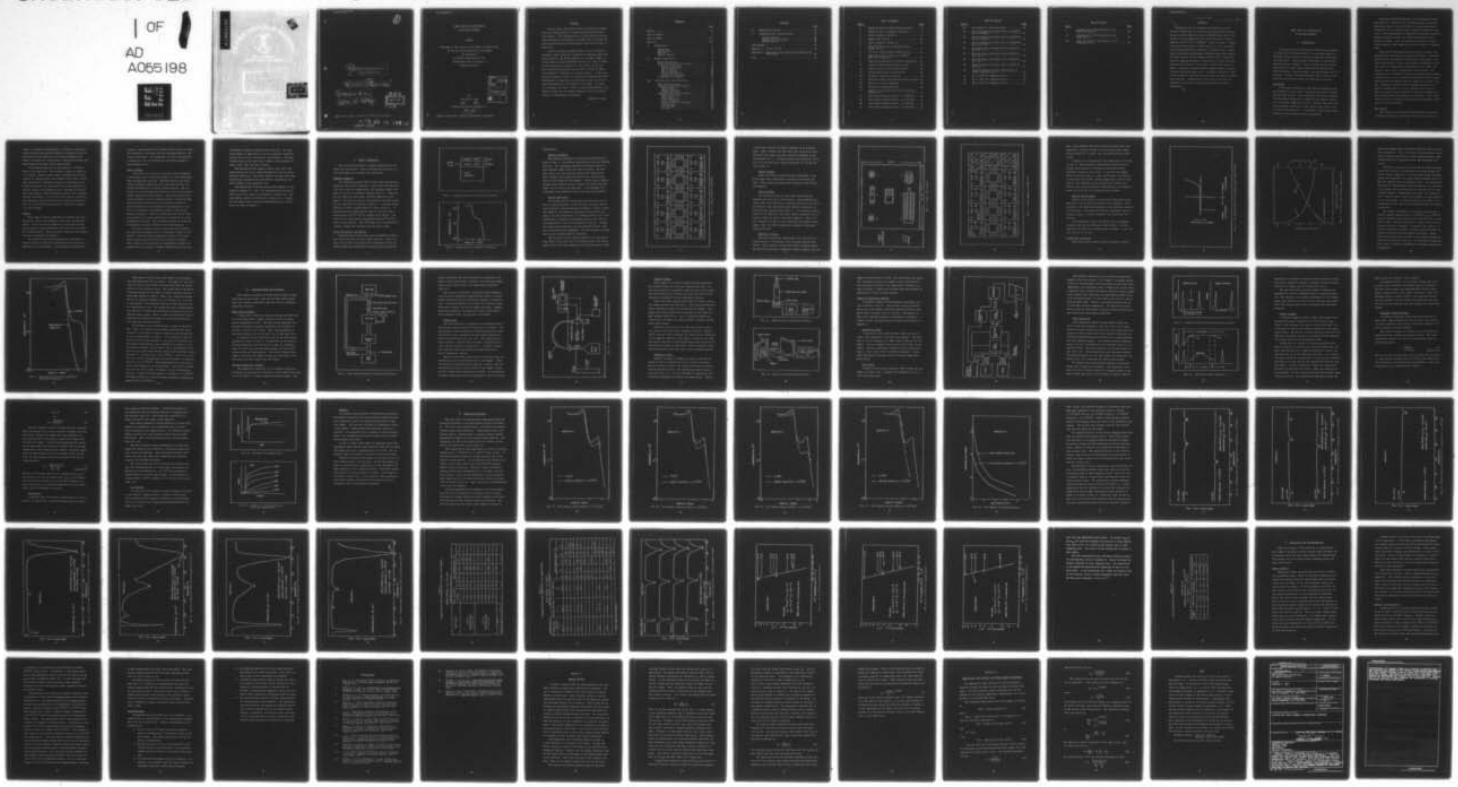

END
DATE
FILMED
7-78
DDC

AFIT/GE/EE/78-4

(1)

(6) DEEP LEVEL TRAP SPECTROSCOPY OF GALLIUM ARSENIDE.

THESIS

(14) AFIT/GE/EE/78-4

(10) Clarence E. Mayo
Capt USAF

(9) Master's thesis,

(11) Mar 78 (12) 82p.

Approved for public release; distribution unlimited.

AFIT/GE/EE/78-4

DEEP LEVEL TRAP SPECTROSCOPY OF GALLIUM ARSENIDE

THESIS

Presented to the Faculty of the School of Engineering
of the Air Force Institute of Technology
Air University
in Partial Fulfillment of the
Requirements for the Degree of
Master of Science

by
Clarence E. Mayo
Capt USAF
Graduate Electrical Engineering

March 1978

Preface

In this study, deep traps induced by electron irradiation were characterized in n-type epitaxial gallium arsenide samples. The characterization of the electron-induced traps was done by calculating the energy levels at which the traps occurred and by calculating the trap concentration of each level.

I wish to express my appreciation to the following individuals, whose technical assistance and guidance made this study possible: My thesis sponsor, Dr. Dietrich Langer of the Air Force Avionics Laboratory (AFAL); Dr. John W. Farmer of the University of Dayton; Mr. Jim Skalski of the Air Force Avionics Laboratory; Captain John M. Borky of AFIT; and Professor J. Lubefeld, my faculty advisor. I wish especially to thank Dr. Elward T. Rodine of the Systems Research Laboratories for spending countless hours (many on his own time) assisting me in all phases of the study. And last, but certainly not least, I wish to thank my grandmother, Mrs. Flowree Linder, for her always inspiring words of self-discipline, encouragement, and wisdom.

Clarence E. Mayo

Contents

Contents

List of Figures

List of Figures

List of Tables

10 to the 14th power/sq.cm.

10 to the 16th power/sq.cm.

Abstract

Trapping states in epitaxial GaAs induced by 1 MeV electron irradiation were measured by transient capacitance. N-type epitaxial GaAs samples with "buffer" layer were irradiated at room temperature with 1 MeV electrons, at doses ranging from $10^{14}cm^{-2}$ to $10^{16}cm^{-2}$. Carrier removal, changes of concentration profile, diode behavior, and C-V characteristics were measured as a function of electron dose. Transient capacitance spectroscopy techniques were used to measure deep trapping levels between $4^{o}K$ and $450^{o}K$. Concentrations of trapping states as a function of electron dose were measured and related to the carrier concentration measurements. The usual electron-induced trapping states with significant variations were noted. Variations of spatial depth of the traps as a function of irradiation and thermal cycling were observed. Samples were in the form of FET test patterns for correlation of material properties and device performance.

DEEP LEVEL TRAP SPECTROSCOPY OF GALLIUM ARSENIDE

I. Introduction

The purpose of this independent study was to characterize deep traps (material defects) in a specific series of epitaxial gallium arsenide samples by Deep Level Trap Spectroscopy (DLTS). Specifically, deep traps in field-effect transistors were analyzed. Other devices such as Schottky barriers, Gunn diodes, impact avalanche and transit time (IMPATT) diodes, varactors diodes, and mixer diodes were not examined. However, the DLTS technique can be used to characterize the material defects in these devices as well.

Background

In the past, luminesence, admittance spectroscopy, and photocapacitance were used to characterize traps in semiconductors (Ref 5:3030). These techniques have been excellent in determining the material properties and chemical identities of shallow traps (0.0-0.5 eV). However, they have been only partially successful in the study of deep traps (0.05-1.1 eV) in semiconductors. In addition, a theoretical understanding of deep traps has been very limited.

Deep Level Trap Spectroscopy is a relatively new technique (Ref 8). Briefly, this technique employs a sensitive capacitance meter, a pulse generator, a dual gated signal integrator, an x-y recorder, and a variable temperature cryostat. From measurements of capacitance transients during a thermal scanning process, the method can observe a wide variety of traps. Also, the apparatus provides a spectroscopic display of the traps plotted as a function of temperature.

Deep Level Trap Spectroscopy has several distinct advantages over the previous mentioned techniques. Since both radiative and non-radiative centers can be observed, it extends trap analysis to deep non-radiative recombination centers missed by luminescence measurements (Ref 7:489). At present, very little is known about these centers. The technique is more versatile than the admittance spectroscopy technique since it is not limited to majority carrier traps. Both minority and majority carrier traps can be easily studied. Finally, the DLTS technique permits observation of traps at energy levels up to 1.1 electron-volts or more. The only large class of traps which DLTS cannot observe are the shallow donors and acceptors nor excitons. Since these shallow centers can easily be detected by luminescence, this is not a serious drawback.

The Problem

The need for quantitative characterization of defects in gallium arsenide is obvious in view of the Air Force in-

terest in compound semiconductors. At present, gallium arsenide exhibits many desirable material parameters (such as high mobility and moderately wide energy bandgap) which makes it suitable for electro-optic, digital processing, and high frequency microwave device applications.

In microwave applications, the quality of epitaxial GaAs is very important. The epitaxial layers are required to be planar, uniform, defect free, and grown with precise control of doping profile and thickness (Ref 1:224). Microwave field-effect transistors, which are majority-carrier n-type structures, are very sensitive to the presence of electron traps in the epitaxial film. Experimental studies have shown that an impurity-related electron trap at approximately four-tenths of an electron-volt from the conduction band adversely affects the microwave frequency characteristics of n-GaAs Schottky barriers and field-effect transistors (Ref 6:2558).

Summary

Deep traps in several semiconductor devices were characterized. Two or more trapping levels were observed per device. Since the devices examined in this study were majority-carrier n-type structures, only deep electron traps were characterized. Minority carrier traps were not studied because of equipment limitations.

The electron traps were manifested as a spectrum of negative peaks in capacitance differences as a function of temperature for each device. This display represented the

change of capacitance due to thermal emission from the traps. The magnitude of each peak was directly proportional to the trap concentration. The temperature at which each peak had a maximum was used to calculate the activation energy of each trapping level.

Plan of Attack

This study was limited to a specific class of samples. An epitaxial layer of gallium arsenide on a semi-insulating GaAs substrate was selected. Schottky barriers and field-effect transistors fabricated from this material were observed and measured for similar characteristics. The uniformity of the metallization patterns as well as the general surface appearances were observed. Many material and electrical parameters (such as doping profiles, current-voltage, and capacitance) were measured to determine uniformity. Selected portions of this material were subjected to a series of irradiations by electrons, using a 1 MeV Van de Graaff accelerator. Electron irradiation was used to introduce defects of a simple nature into the material at a prescribed rate and dose. This provided a method to study the relationship of simple defects to device performance.

The basic procedure used in this study was to monitor the capacitance changes across the depletion regions of the devices. This was done by applying a reverse bias across these regions, by providing one or two positive pulses across them, and by observing the capacitance transient associated with the return to thermal equilibrium of the level

following an initial non-equilibrium condition. The transient change of capacitance across the depletion region described the rate of electron-hole recombination. The exponential decay of the capacitance transient was measured for shape, size, sign, and time constant.

The gallium arsenide samples used in this study were fabricated by the Device Technology Branch of the Air Force Avionics Laboratory. With these samples the Deep Level Trap Spectroscopy experiment was performed to characterize the defect states in the epitaxial film.

The preparation of the gallium arsenide samples is presented in Chapter II. Next, the instrumentation and procedures used in the study are presented in Chapter III. The experimental results are discussed in Chapter IV. Finally, the conclusions are stated and recommendations for further study are made in Chapter V.

II. Sample Preparation

The following discussion of sample preparation is divided into three parts. These are substrate material, device fabrication and testing, and irradiation.

Substrate Material

The substrate material used in this study was chromium doped gallium arsenide (GaAs:Cr). Since this starting material had a very low conductivity, two epitaxial layers were grown on top of the substrate material (Fig. 1). These layers were grown by vapor phase epitaxial deposition techniques. The material used in the deposition of these layers was tin doped gallium arsenide (GaAs:Sn). A typical doping profile for these sandwich layers is shown in Fig. 2. It was estimated from this profile that the top layer had a concentration of 10^{16} cm^{-3} to a depth of one micron. The second layer concentration was approximately 10^{15} cm^{-3} at three to four microns. The 10^{15} layer can be considered as a buffer between the substrate and the active layer.

Device Fabrication and Testing

Schottky barriers and field-effect transistors (FET's) were fabricated from the multi-layer material. Ohmic contacts were provided for electrical connections and Van der Pauw patterns were fabricated for mobility and resistivity

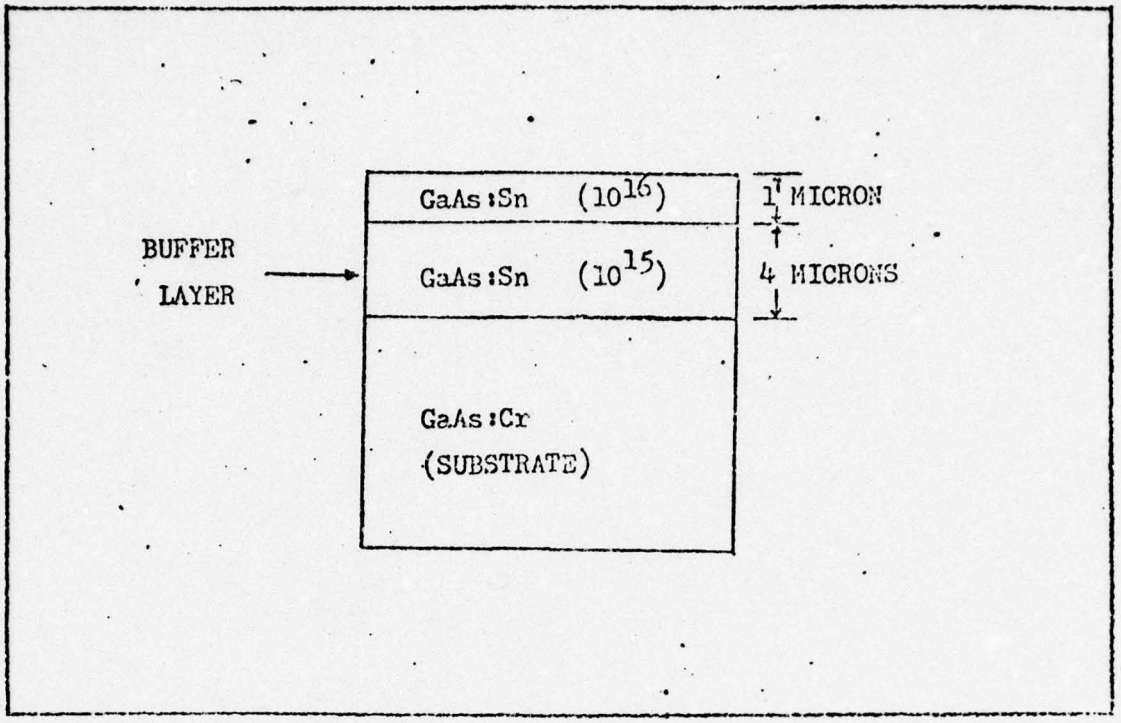

Fig. 1. Substrate Material With Epitaxial Layers.

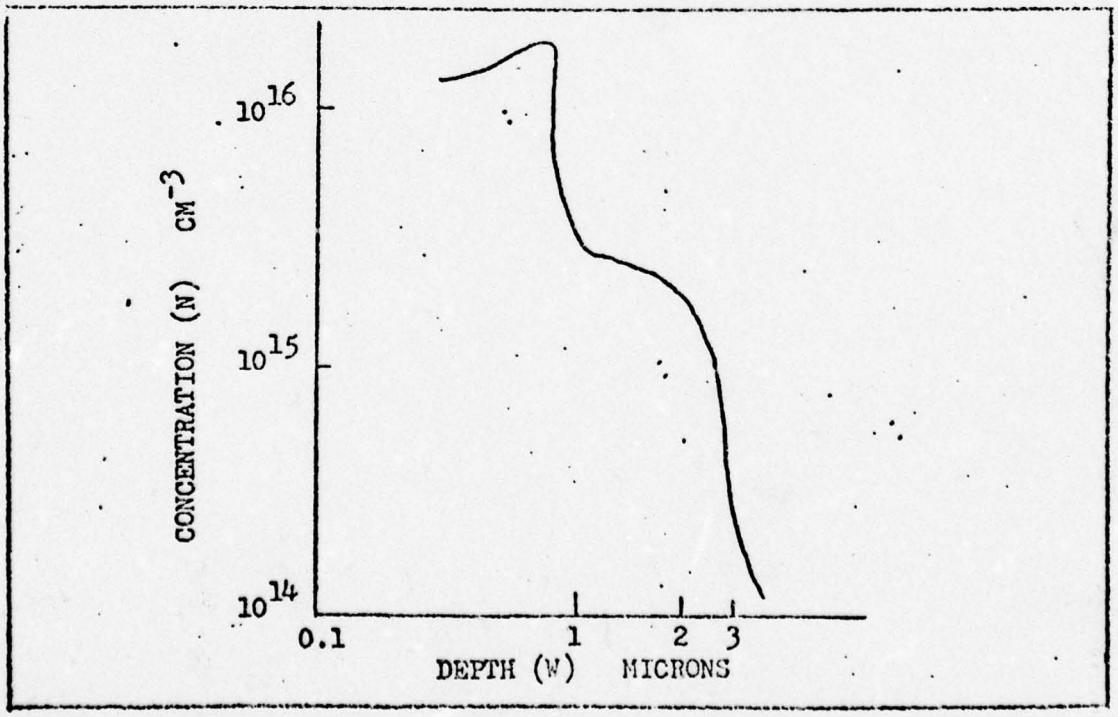

Fig. 2. Doping Profile of Sandwich Materials.

measurements.

Geometric Patterns

The geometric patterns for the devices fabricated are shown in Fig. 3. The devices labeled number two are Schottky barriers. The rectangular patterns with small squares in them (labeled number three) are ohmic contacts. Devices four, five, six, and seven are field-effect transistors. These (larger than normal) FET devices were specifically made for this study as test samples. Device four is approximately three times the area of device five and nearly six times that of devices six and seven. The remaining four rectangular pads represent the Van der Pauw test patterns.

Device Fabrication

The devices used in this study were fabricated by the Device Technology Branch of the Air Force Avionics Laboratory using well known processing techniques. Briefly, masks were made for the geometric patterns and photoresist was spun on the GaAs substrates. The desired patterns were then obtained by a process of selectively exposing and etching the photoresist on top of the substrate material. Finally, the metallization patterns for each Schottky barrier, FET, and ohmic contact were deposited. All devices were on mesas five or more microns high for isolation.

The Schottky barrier device consisted of a gold-germanium ohmic contact pad next to an aluminum pad. The field-effect transistors were composed of two gold-germanium ohmic

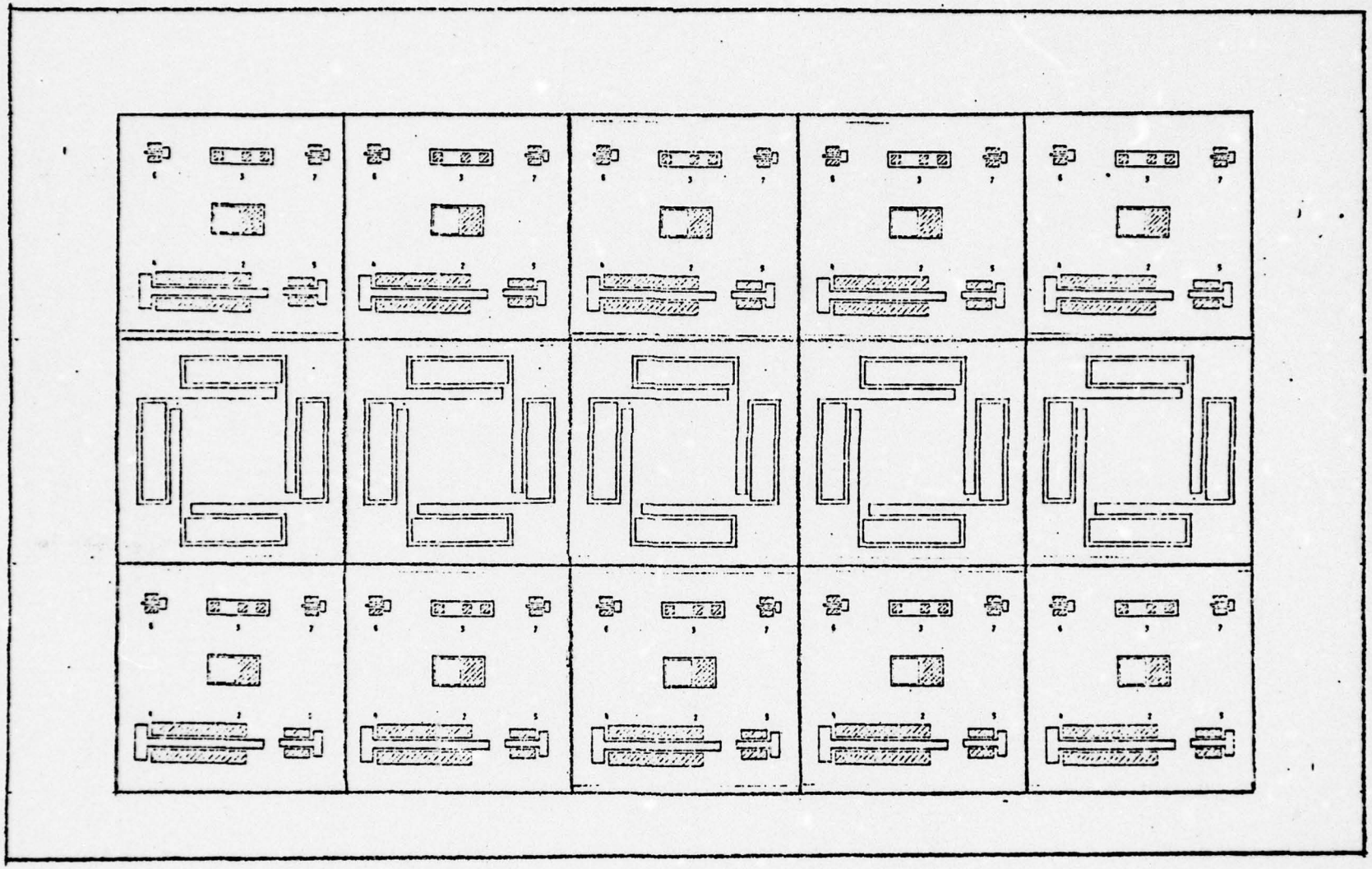

Fig. 3. Device Geometric Patterns.

contact pads (source and drain) separated by an aluminum gate. Ohmic contacts and Hall pads (four point probe test patterns) were gold-germanium, alloyed in hydrogen at approximately 400° C. A sample pattern with dimensions of 0.2 cm by 0.2 cm shows these various materials for several devices (Fig. 4).

Device Testing

After the various devices had been fabricated on the multi-layer GaAs, preliminary testing of each device was done. This testing included visual inspection and electrical analysis.

Device Mapping

The structural shape of each wafer fabricated was sketched with the aid of a microscope. These drawings provided a map of the location of specific devices on the wafer. In addition, each test pattern was labeled numerically to assist in the identification (Fig. 5). For instance, device label R9-2-4 meant that this field-effect transistor was located on wafer R9, die 2, and device number 4. Also, surface defects or anomalies were identified and marked accordingly. Once the device mapping was completed, electrical testing was done.

Electrical Testing

Since most electrical testing had to be done with microprobes under a microscope, only the large devices were tested. This included the Schottky barriers labeled number two and the field-effect transistors labeled numbers four and

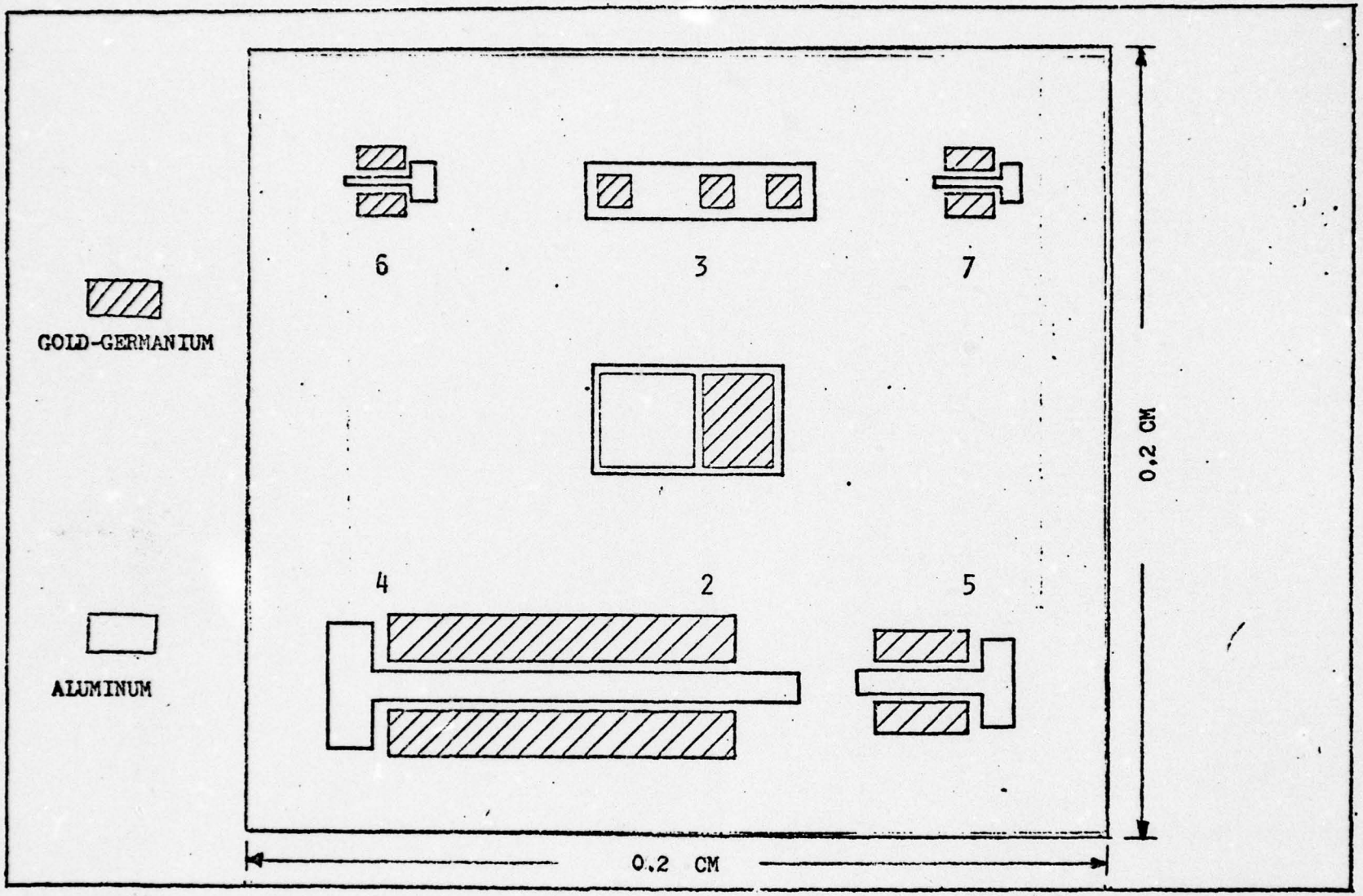

Fig. 4. Sample Test Pattern

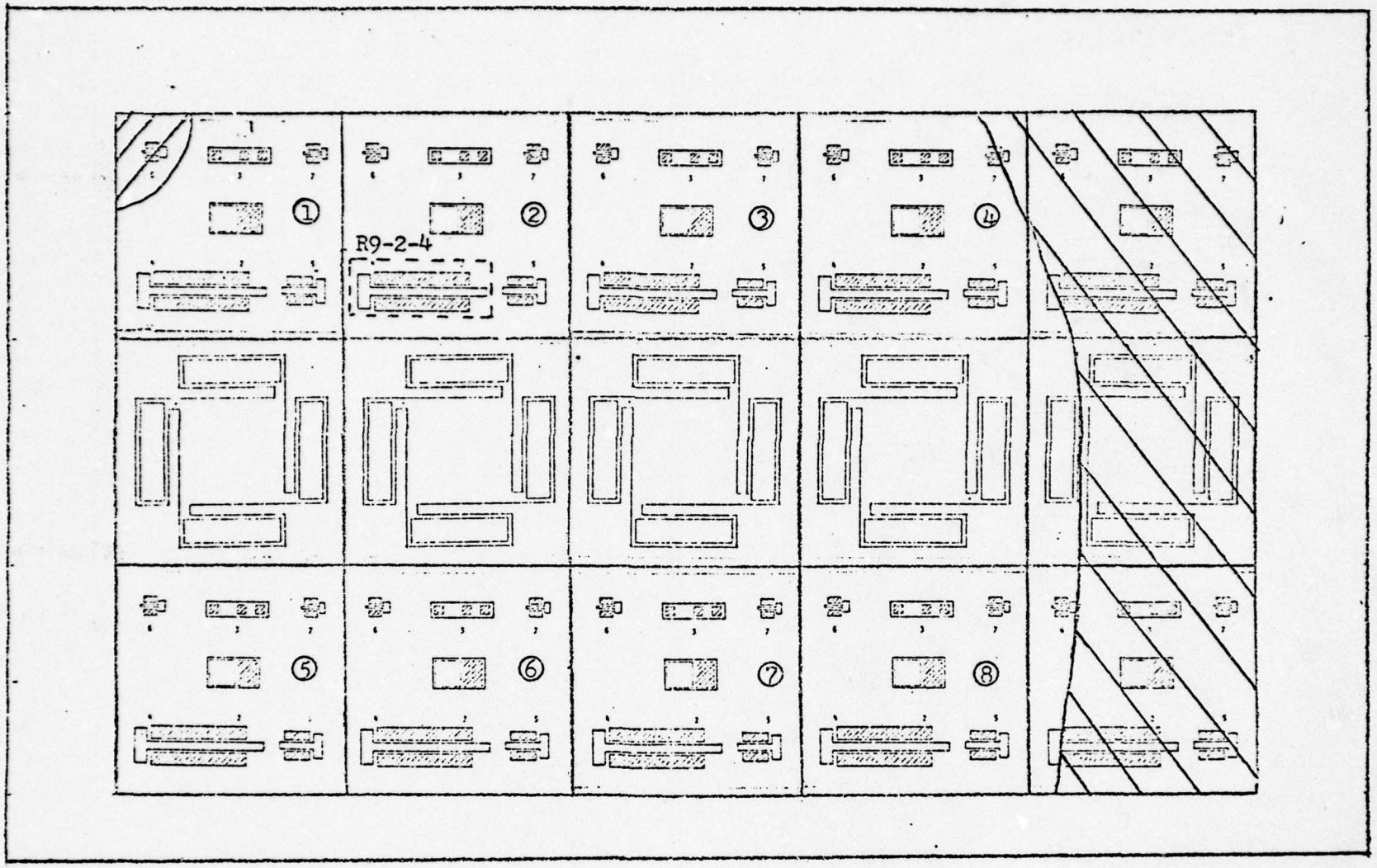

Fig. 5. Device Mapping of Wafer R9.

five. Data gathered from these devices included zero bias capacitance, current-voltage (I-V) characteristics, capacitance-voltage (C-V) curves, and concentration-depth (N-W) curves.

A typical I-V characteristic for sample R9-2-5 is given in Fig. 6. This particular field-effect transistor had a forward bias breakdown of nearly 0.6 volts and reverse breakdown voltage of -20.0 volts. A C-V plot for sample R9-9-5 is shown in Fig. 7. Also, $1/C^2$ versus V is plotted to determine the device's barrier height (0.8 volts in this case) at the intercept of the reverse bias voltage axis. Devices with uniform electrical characteristics and measurements were selected to be diced and later bonded.

Bonding and Packaging

Devices to be used in the Deep Level Trap Spectroscopy experiment were eutectically bonded to TO-5 headers. This amounted to the permanent placement of the substrate material on the header. Some benefits from this attachment were mechanical support, thermal conduction, and electrical connection.

Interconnection between the devices and the package terminals was done by ultrasonic wire bonding. Aluminum leads (0.0254 mm thick) provided ohmic contacts, to the various devices on the die.

Irradiation of Samples

Fabricated samples which had been inspected, electri-

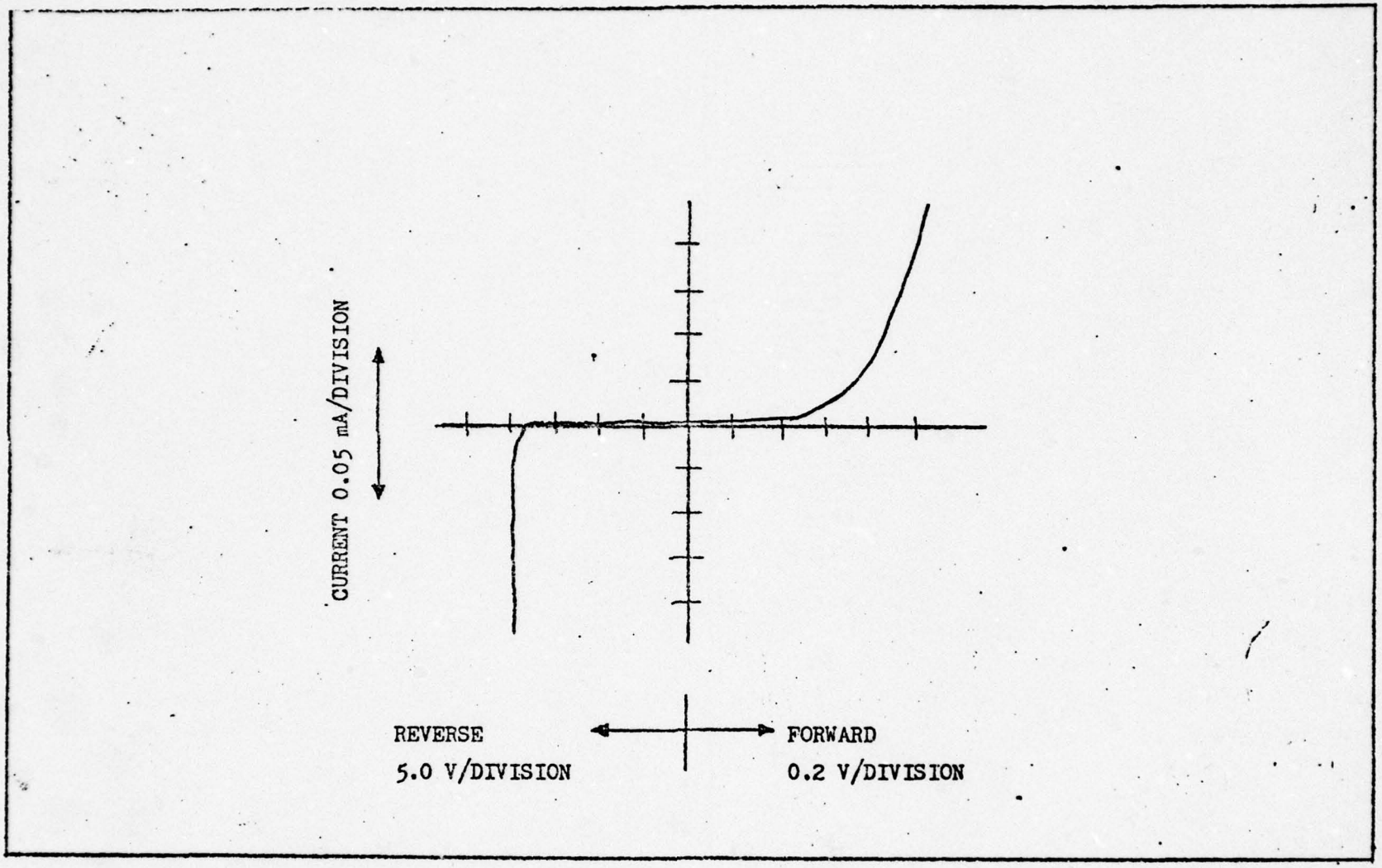

Fig. 6. I-V Characteristics of Epitaxial GaAs, Sample R9-2-5.

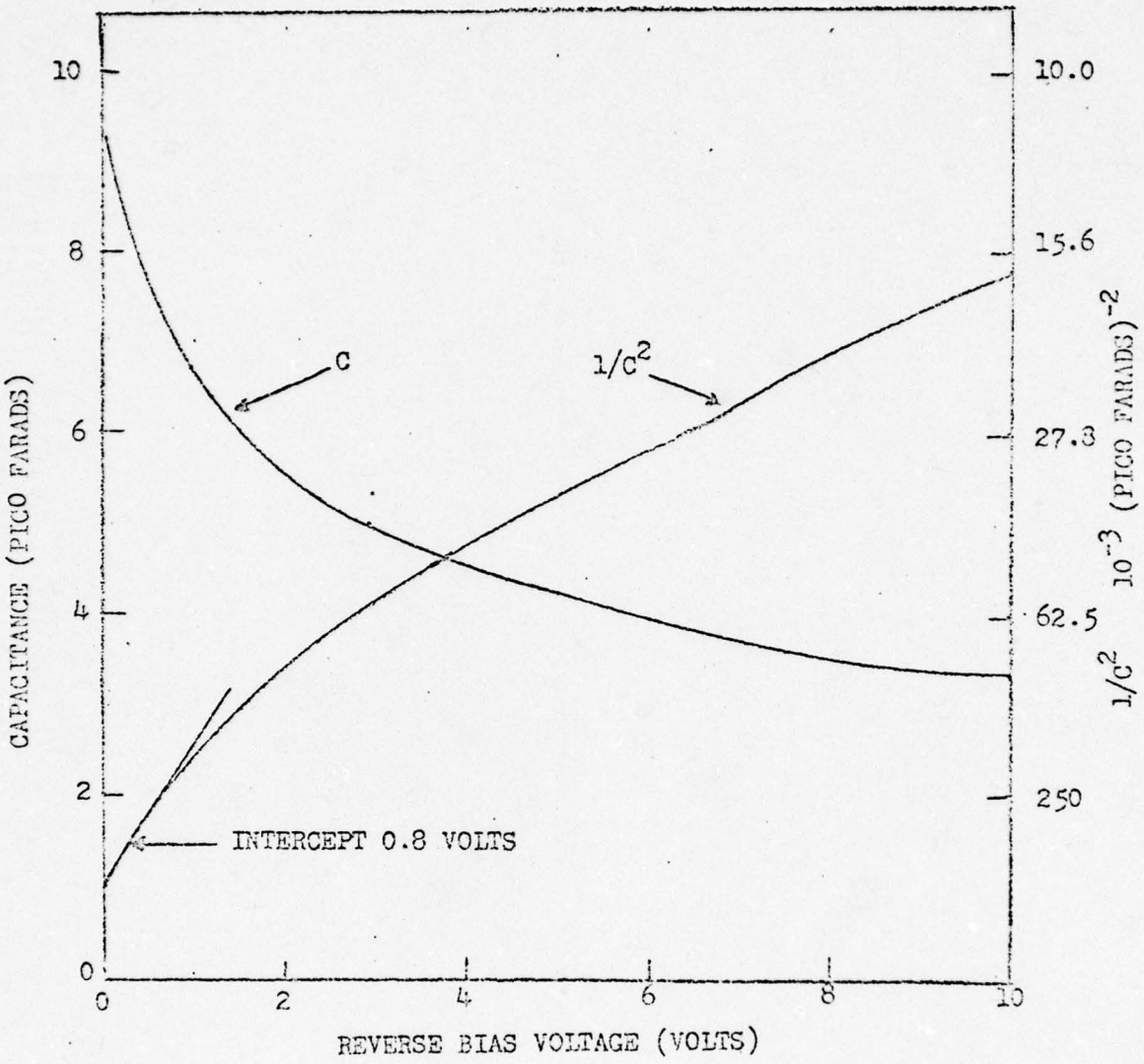

Fig. 7. C-V Plot, GaAs Epitaxial Sample R9-9-5.

cally and packaged were irradiated using the Model JS Electron Accelerator. This 1 MeV Van der Graaff electron accelerator consists essentially of three operating parts: high voltage generator, accelerator tube, and associated circuitry.

Basically, the operation of the Van de Graaff electron accelerator involves the generation of a high voltage (10^6 volts) across a capacitor. From the high voltage terminals across this capacitor, very high energy electrons (0.75-1.0 MeV) are emitted into an accelerator tube. The accelerator tube with its electrostatic field accelerates the electrons to an energy level determined by the potential of the high voltage terminal. Subsequently it focuses the electrons into a beam and then carries them through the tube extension to the exit portal. At the exit portal, the target to be irradiated is then subjected to controlled doses of electron irradiation.

The samples irradiated in this study were exposed to electron dosages ranging from $1 \times 10^{14}/cm^2$ to $1 \times 10^{16}/cm^2$ with corresponding flux densities of $0.03\mu A/cm^2$ and $1.10\mu A/cm^2$ at 1 MeV. Material defects of a simple nature were introduced by electron damage. In essence, the stream of electrons striking the sample's surface creates sporadic vacancies in the material crystalline structures. These structural changes were observed in the sample's doping profile after irradiation (Fig. 8). The variation of this profile from the original concentration and depth measurements is apparent.

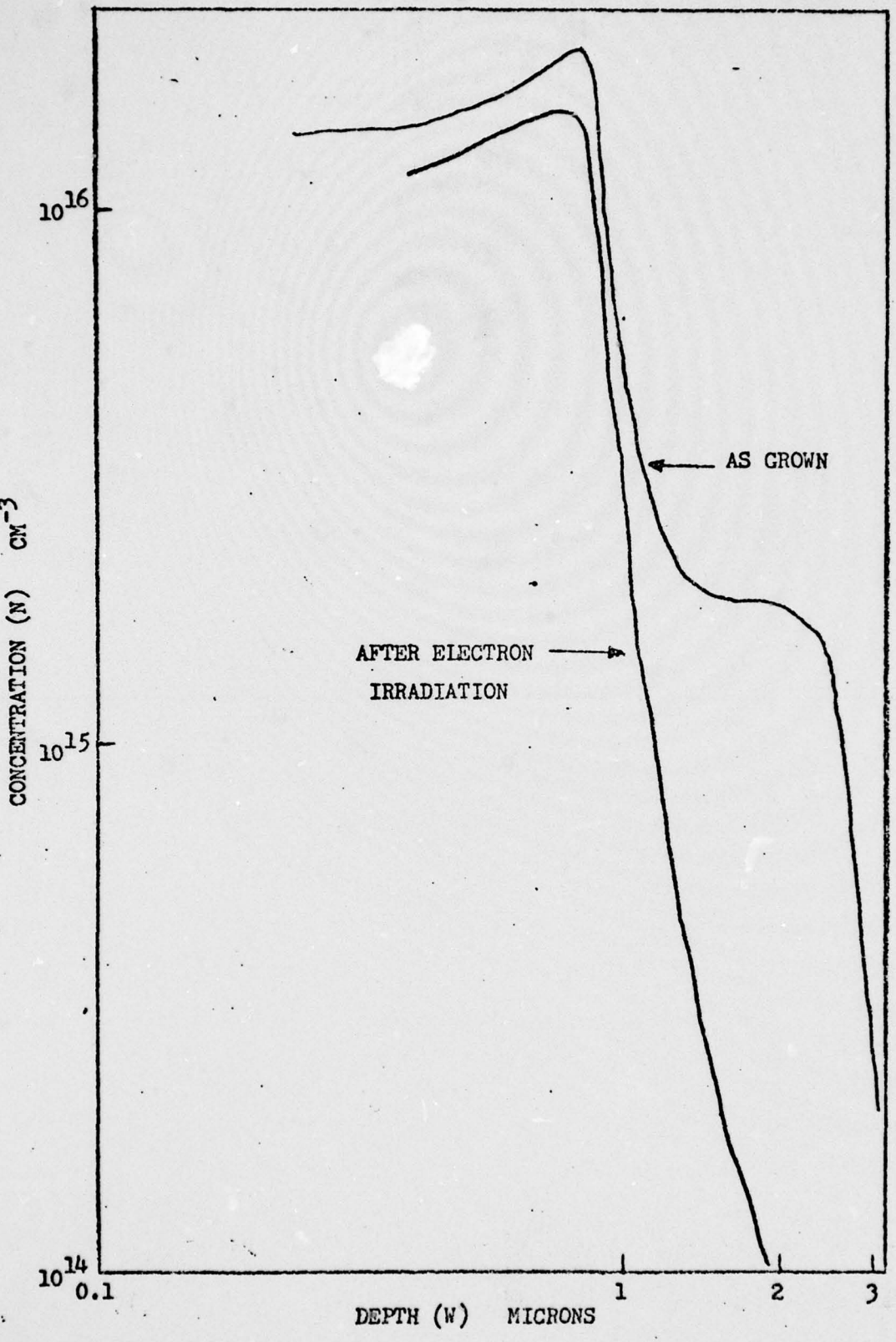

Fig. 8. GaAs Sample R9-2-4 After $5X10^{15}CM^{-2}$ Electron Irradiation.

Some comments are in order with regard to the electron dose and production rate of defects. The range of 1 MeV electrons in GaAs is about 1000μ which has many times the thickness of the 4μ epitaxial layer. The energy loss of electrons traveling through the epi layer is nearly constant and also very small ($dE/dx \sim 0.7$ keV/μ). Thus, after traveling through the 4μ of epitaxial material, $dE = 0.7$ keV/μ X 4μ = 2.8 keV, so the energy of the electrons arriving at the substrate will be 1 MeV minus 2.8 keV. The energy loss rate is approxmately the same for Al because the densities of electrons in Al and GaAs are nearly equal. Hence, it does not matter that the irradiation was performed through the Al Schottky gates which were less than one micron thick.

The threshold for ion displacement in GaAs is about 400 keV. Hence, the energy of the incident beam was well above threshold. The number of defects created by this irradiation is not a simple number to obtain. If we consider a layer of material that is thin compared to the range of electrons and a beam energy significantly above threshold, the number of displacements is simply $\sigma N_a \phi$, where σ is the displacement cross section, N_a is the atomic density and ϕ is the electron fluence. For GaAs, $\sigma = 65$ barns, $N_a = 4.4 \times 10^{22} cm^{-3}$. Hence for a fluence of 5×10^{15} electrons/cm^2, the maximum number of displacements is $14.5 \times 10^{15} cm^{-3}$. Each displacement can cause two defects (one vacancy and one interstitial). The carrier removal rate and the total number of vacancies in the un-irradiated material. Hence, for these samples, a fluence of $5 \times 10^{15} cm^{-2}$ can easily result in a carrier removal and defect introduction greater than $5 \times 10^{15} cm^{-3}$.

III. Instrumentation and Procedures

This chapter discusses the three major systems of apparatus used in this study. They are the high vacuum equipment, the variable temperature cryostat, and the transient capacitance network.

High Vacuum Equipment

A vacuum of 1.0 micron of mercury (μm Hg) or better had to be obtained before a sample could be cooled to liquid helium temperature (4.2°K). The high vacuum equipment used was made by National Research Corporation and designed to provide a vacuum to 10^{-3} μm Hg. Thus, this equipment was more than adequate for its use with the cooling apparatus.

A schematic of the functional units of the high vacuum equipment is shown in Fig. 9. As indicated in the diagram, the most important units are the fore pump, the diffusion pump, the cold trap, the ionization gauge, and the various vacuum valves and thermocouples. The vacuum equipment provided a vacuum for the sample through its connection to the heli-tran unit which housed the test sample.

Variable Temperature Cryostat

The temperature dependence of the trapping states was determined by sweeping the temperature of the sample from about 4.2 °K to 450°K in a liquid transfer heli-tran system. This

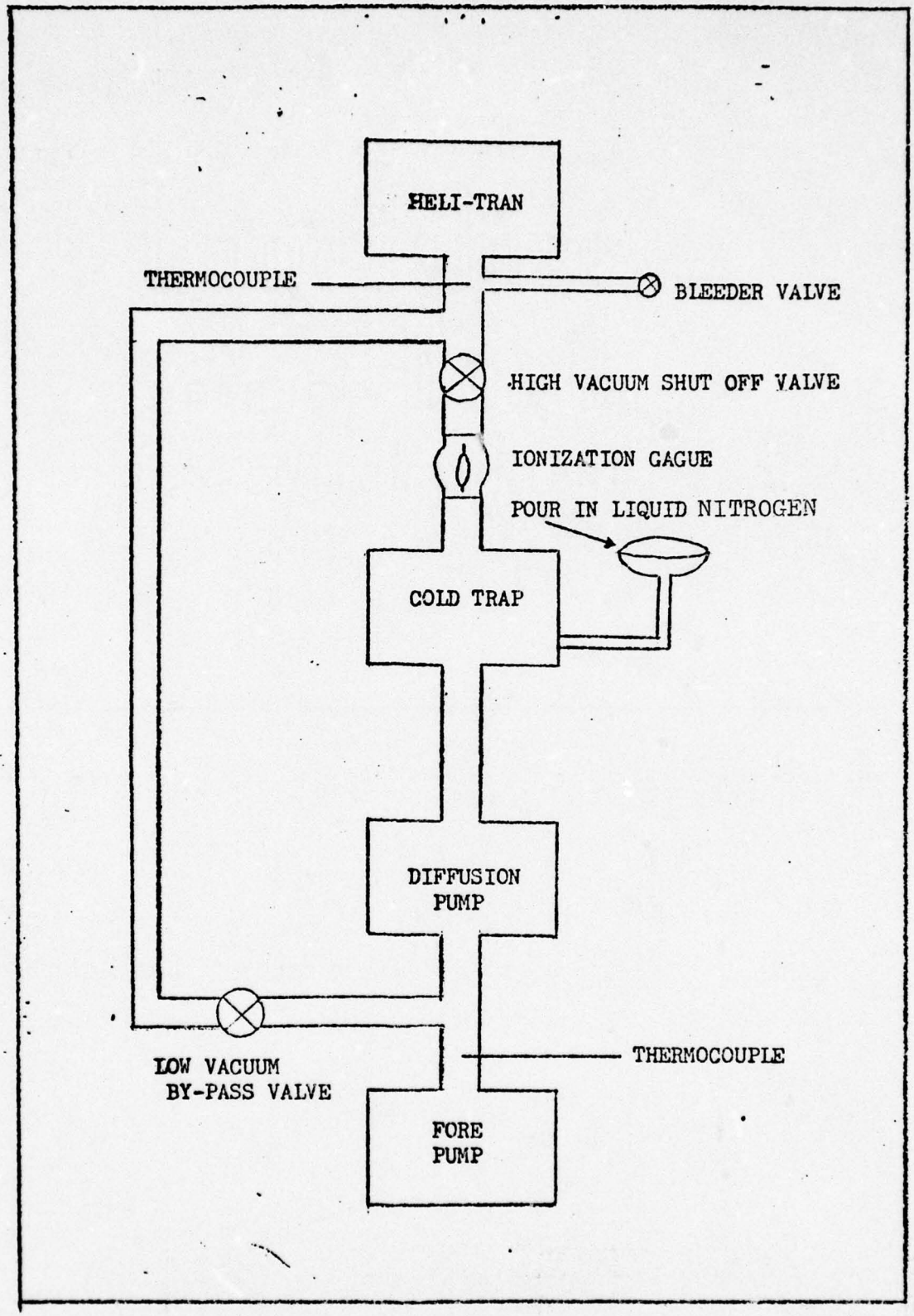

Fig. 9. High Vacuum Equipment Functional Connections.

system, which was made by Air Products and Chemicals, consists of dewar attachments, transfer line, heli-tran sample holder, flow control panel, and temperature controller (Fig. 10).

The variable temperature cryostat provided refrigeration from room temperature (approximately 300°K) to liquid helium temperature by the controlled transfer of liquid helium. The helium flowed at a constant rate through a high efficiency transfer line to the sample interface. Temperatures were gradually increased from 4.2°K to 450°K with a heater wrapped around the heli-tran cold finger.

Thermocouple

The broad variation of temperature was measured with a thermoccuple mounted inside the heli-tran cold finger. The thermocouple, which consisted of chromel-gold material with 0.07 atomic % iron, indicated the test sample temperature with an estimated precision of 0.1°K. The reading was obtained through a circuit which provided a relationship between thermal voltage and temperature. A digital temperature indicator with four significant digits provided a direct temperature readout.

Errors in the sample temperature are possible since the thermocouple was not mounted exactly on the sample. Physical limitations prevented such mounting. However, with the thermocouple located in the vicinity of the sample, fairly accurate temperature readings were obtained. An explanation of sample temperature errors is presented in the conclusions.

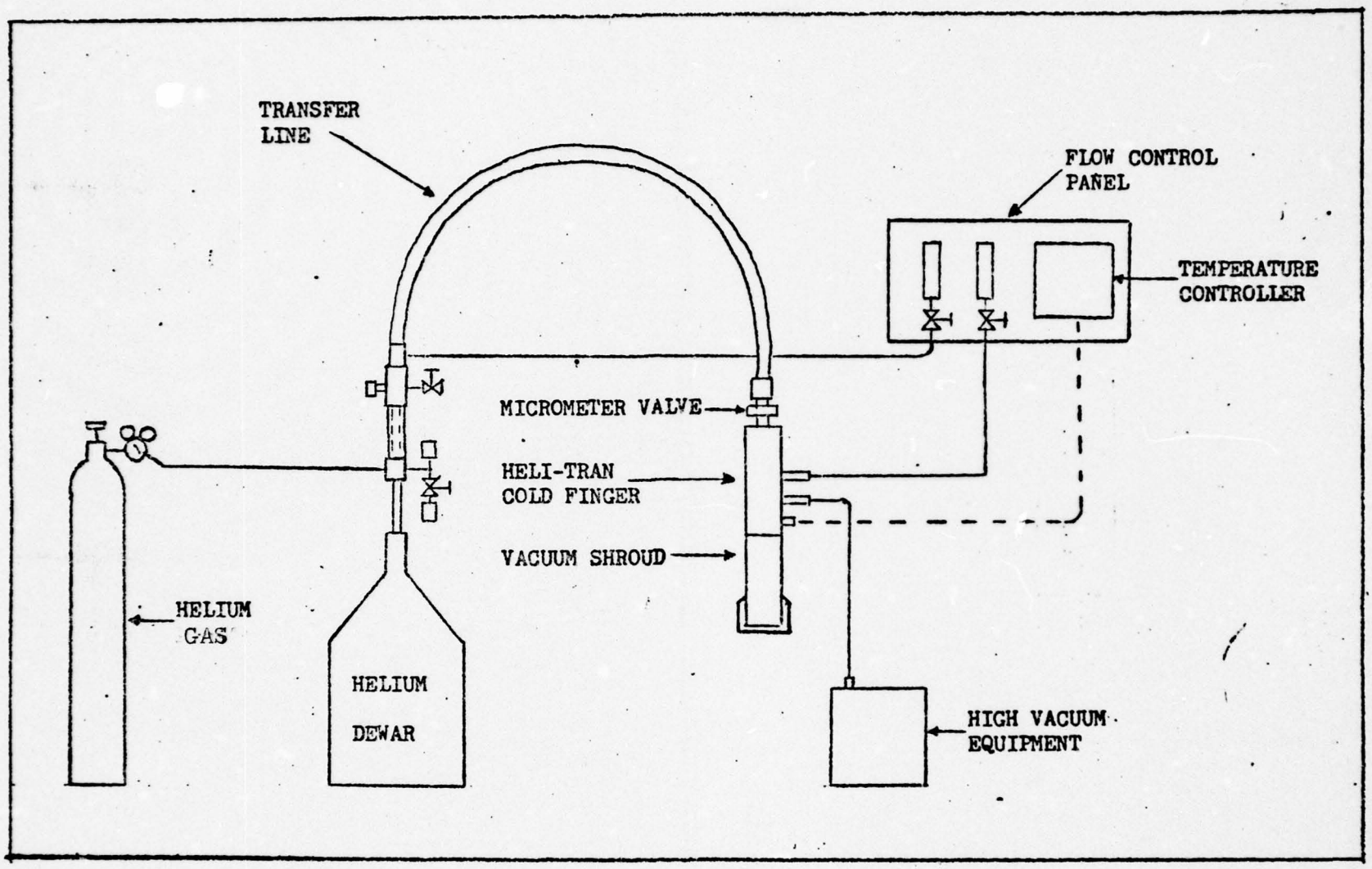

Fig. 10. Variable Temperature Cryogenic System.

Sample Mounting

Each sample to be cycled through the DLTS experiment was mounted inside the heli-tran vacuum shroud (Fig. 11). The vacuum shroud in conjunction with the high vacuum equipment and liquid helium transfer flow provided the required cryogenic environment for low temperature testing.

Teflon tape was wrapped around each TO-5 header before the sample was put into the holder. This tape provided electrical insulation between the holder and the header. The sample was snugly fitted into an opening in the holder for good thermal conductivity. Also, a radiation shield was lowered over the sample to reduce radiative emission during temperature sweeps.

Electrical connections were made from the TO-5 exterior posts to the metal plate terminals (Fig. 12). Specifically, the post which connected the ohmic pad was connected to the negative terminal of the plate. Similarly, the other post which connected the gold-germanium pad was connected to the positive terminal of the plate. These connections were soldered and wire leads were used as the connecting medium.

Temperature Sweep

Gradual increases in temperature above 4.2°K were obtained by using a combination of flow control and heater power to conserve helium. By closing the shield flow meter and the micrometer valve, the temperature could be slowly increased (Fig. 10). Greater increases in temperature were obtained by gradually increasing the heater power. After a

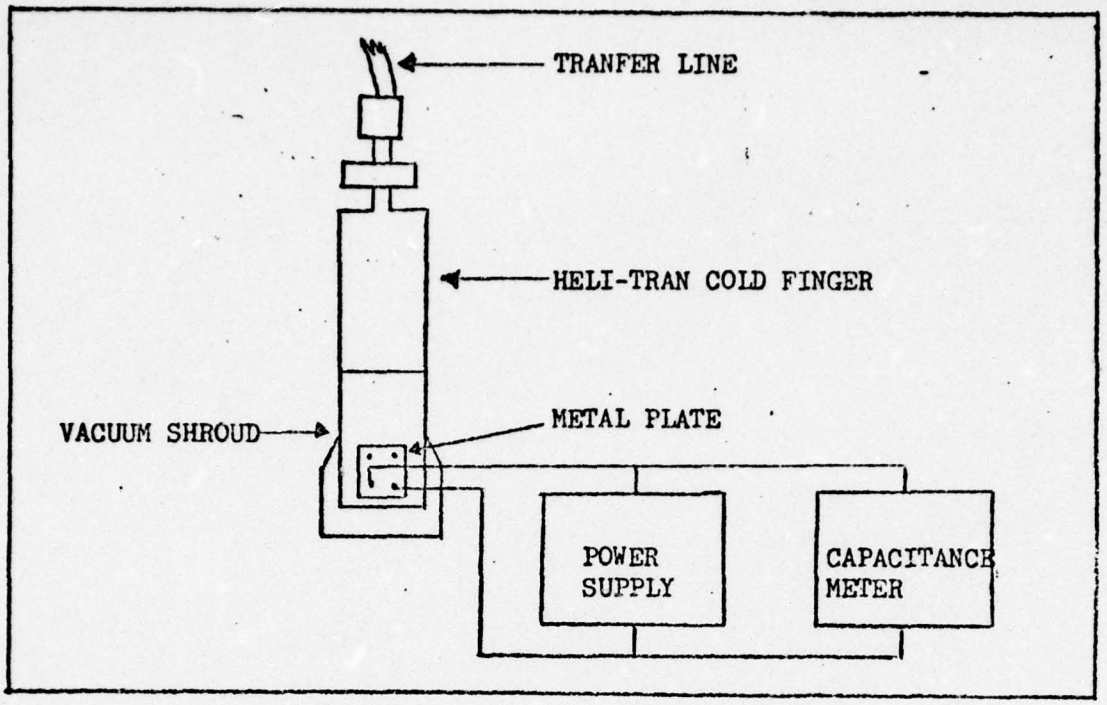

Fig. 11. Sample Mounted Inside Vacuum Shroud.

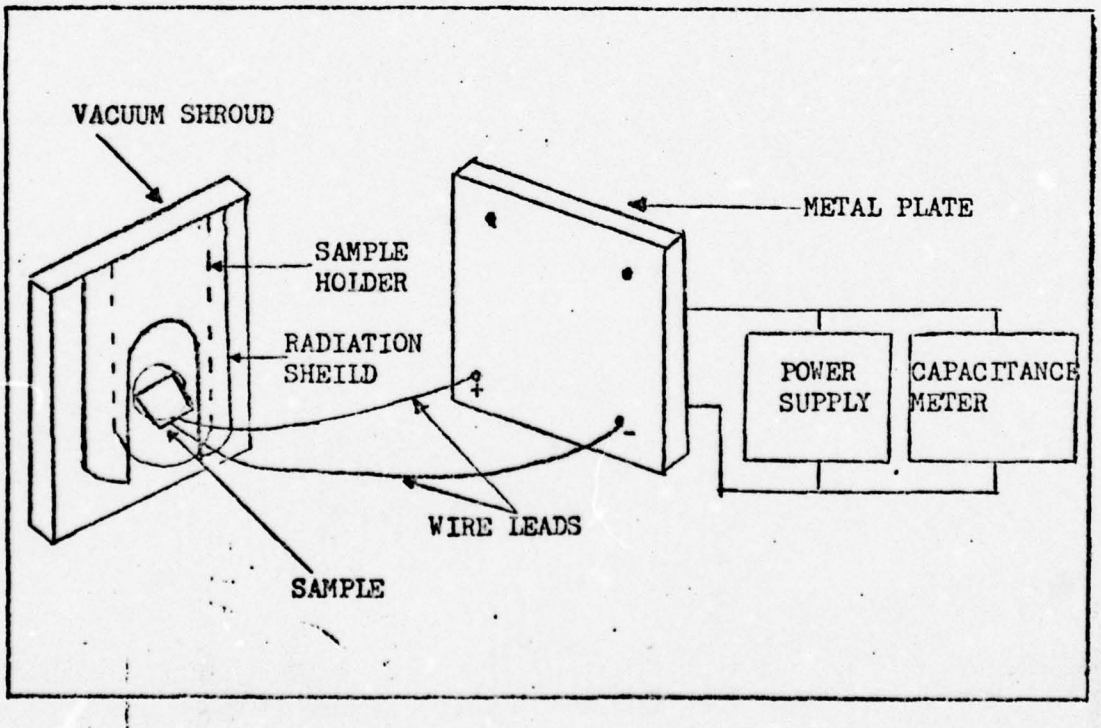

Fig. 12. Wiring Connections To Metal Plate.

sample had been heated to 450°K, the heater power was turned off. Usually, the heli-tran sample holder was allowed to cool naturally to ambient room temperature. However, on some occasions, a sample was re-cooled much more quickly by repeating the helium transfer process.

Transient Capacitance Network

A schematic diagram of the transient capacitance network is shown in Fig. 13. This network consists of pulse generators, bias supply, sensitive capacitance meter, dual gated boxcar averager, and x-y recorder. The physics of Deep Level Trap Spectroscopy is capacitance transients. A summary of the underlying physics of DLTS is presented in Appendix A.

Capacitance Meter

A capacitance meter (Boonton Model 72BD) was used to measure the capacitance across the test samples. The meter uses a carrier frequency of 1 MHZ at 100 mV RMS as its test signal. It has a response time of less than 2 msec for all ranges. The four capacitance ranges have full scale readings of 2.000, 20.00, 200.0, and 2000 picofarads. A four digit LED display provided quick and accurate capacitance measurements.

Bias Supply

A direct current power supply was used to keep the test sample in reverse bias. Typical bias voltages of -3.0 to -10.0 volts were used.

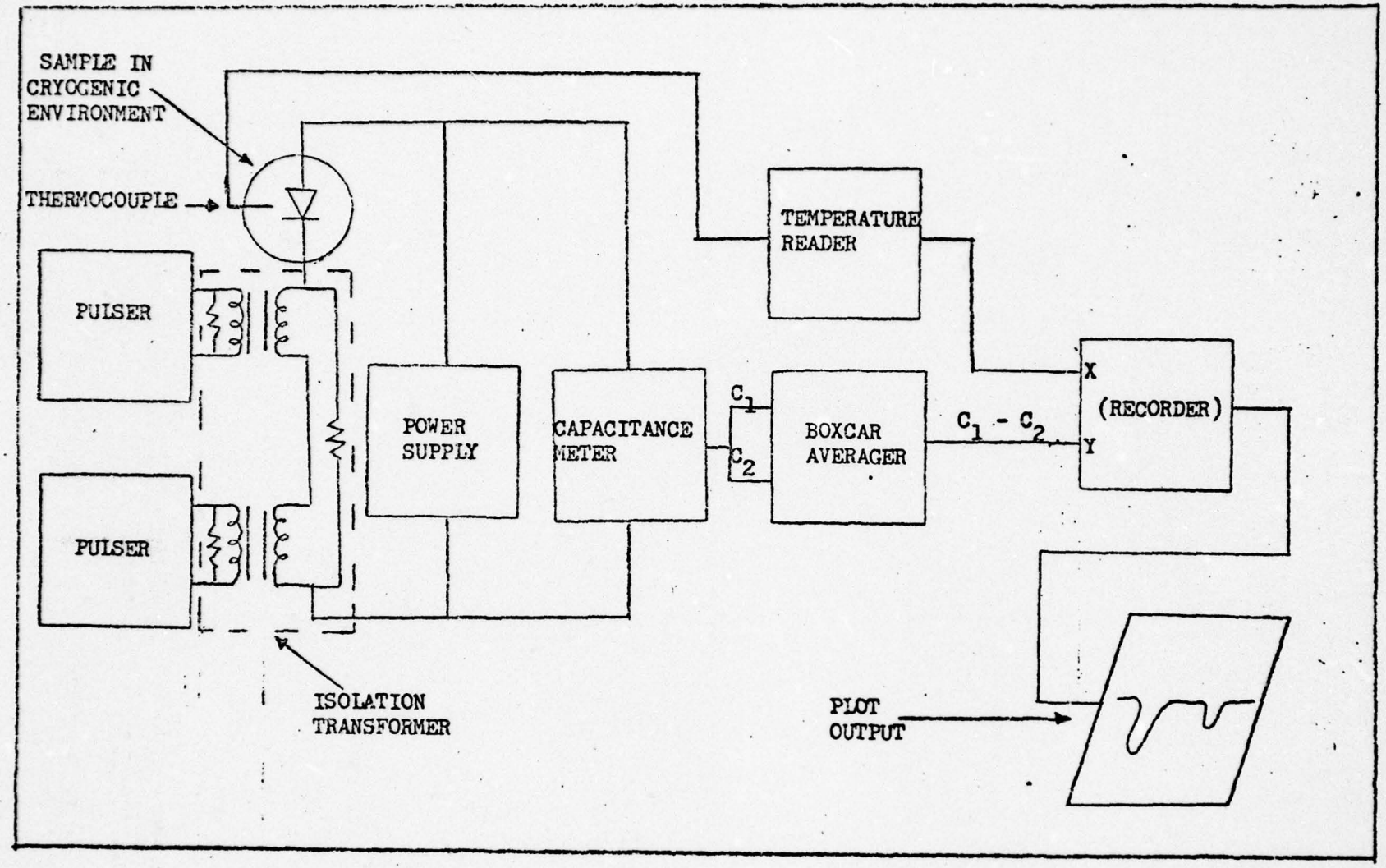

Fig. 13. Transient Capacitance Network.

The intrinsic capacitance of the depletion region depended on the bias voltage. For example, a Schottky barrier could have a capacitance of 60 picofarads at zero bias and a capacitance of 5 picofarads with a reverse bias of ten volts. A negative bias increased the sample depletion region's width, since reverse bias capacitance is approximately $\epsilon A/W$, where ϵ is the permittivity, A is the device area and W is the depletion layer width. However, increasing reverse bias led to decreased junction capacitance. Non equilibrium conditions across the test samples (mounted inside the heli-tran) were obtained by using pulse generators.

Pulse Generators

Pulse generators (Hewlett Packard Model 1900A) were used to make rapid changes in the bias of the test sample. Injection pulses momentarily drove each test sample from its quiescent reverse-biased state into forward conduction and introduced majority carriers (electrons for n-type material) into the depletion region. The injection pulses resembled spikes (10 μsec in duration) with an amplitude equal to the quiescent bias. The pulse repetition period was usually 70 msec (Fig. 14). Pulse transformers were connected between the pulse generators and the test sample for electrical isolation (Fig. 13), preserving the desired pulse shape.

The sudden bias voltage change produced a capacitance change and a capacitance transient. The capacitance transient was due to thermal emission of trapped changes in the space charge layer next to the junction or barrier (Ref 8).

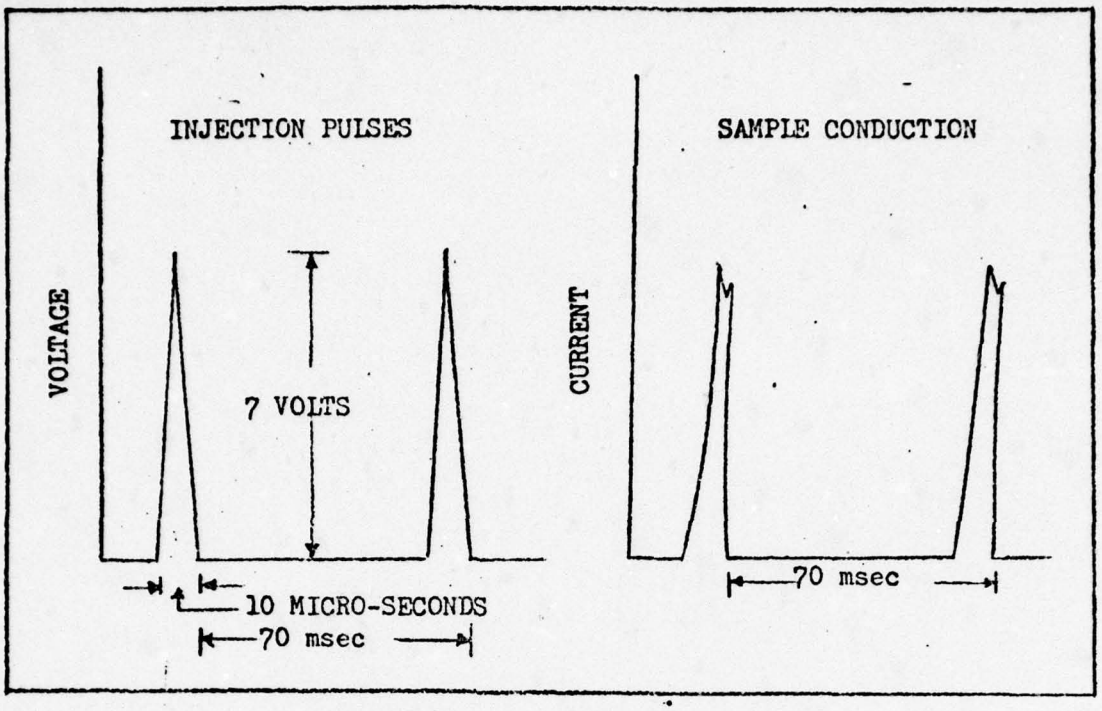

Fig. 14. Injection Pulses and Resultant Current Pulses.

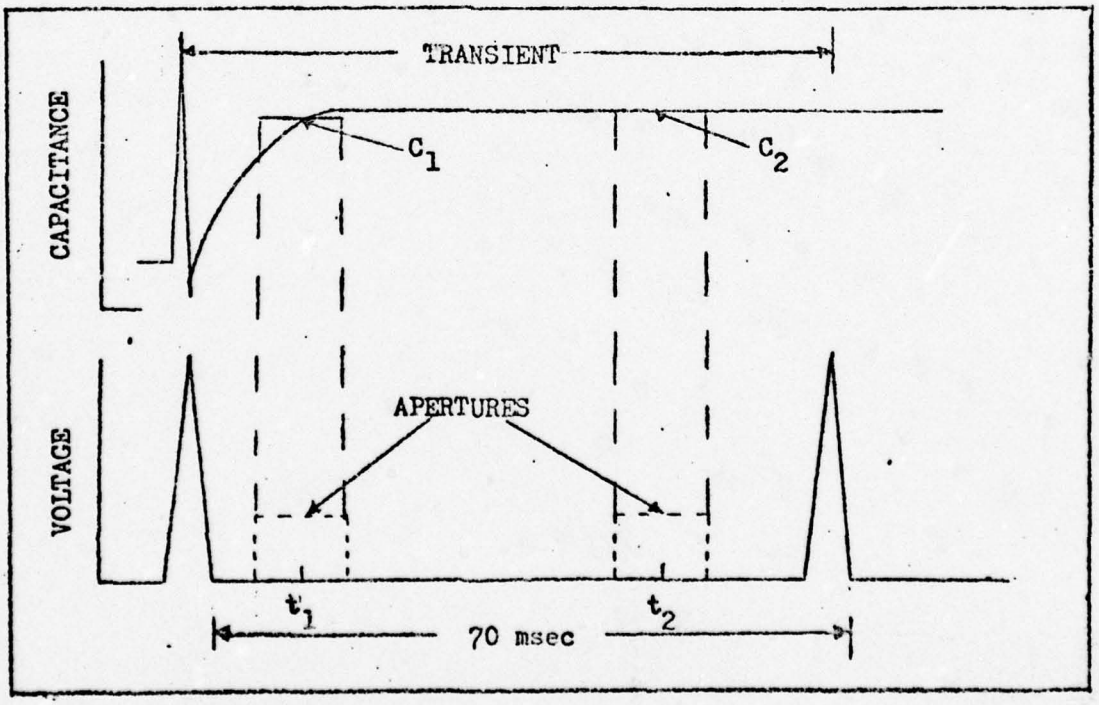

Fig. 15. Position of Boxcar Apertures.

Basically, the capacitance changes resulting from the injection pulses caused the average occupation of trap levels by electrons to change from the steady-state value.

The injection pulse provided a means of filling and emptying the electron trapping states in a controlled manner. The changes in the electron occupation of the trapped states were observed by monitoring the junction capacitance after the injection pulse and by analyzing the associated transient.

Boxcar Averager

A Princeton Applied Research (Model 162) double boxcar averager with gated integrators was used in this study. Simply, this instrument was used to selectively sample and to average the capacitance transient detected by the capacitance meter. The process involved repeatedly measuring the amplitude of specific points on the transient and computing the average value of the measurements taken.

Pulses from the output of the pulse generators were used as triggers to activate the boxcar apertures (Fig. 15). Since these pulses had a repetition period of 70 msec, the apertures had to be set within this interval. As a result, the gate settings of the apertures (t_1 and t_2) were normally positioned at 5 msec and 50 msec respectively from the trigger signal. The time permitted to sample the capacitance transient of each gate was 5 msec. Thus, the averaging of the transient over this interval produced the averaged capacitances C_1 and C_2. The capacitance difference (C_1-C_2) was

then used as the Y-input to the recorder.

An essential feature of the boxcar averager was the ability to set an emission rate window (aperture settings) such that the averager only responded when it saw a capacitance transient with a rate within the window. Thus, the equipment showed a response peak at the temperature where the trap emission rate was within the window when the emission rate of the trapping state was changed with temperature sweeps.

Transient Network Settings

A variety of transient network settings were used in this study. Many experimental runs were made under different bias conditions, with various capacitance readings, and with a variety of boxcar settings.

The boxcar settings were changed to produce different capacitance time constants and emission rates. The capacitance time constant for each run was calculated from the following equation:

$$\tau = \frac{t_1 - t_2}{\ln(t_1/t_2)} \qquad (1)$$

(Appendix B)

where t_1 is the time for gate 1 and t_2 is the time for gate 2. The electron emission rate for each run was obtained as the reciprocal of the capacitance time constant. Thus, the emission rate e_R is given by the relation:

$$e_R = \frac{1}{\tau} \tag{2}$$

or

$$e_R = \frac{\ln(t_1/t_2)}{t_1 - t_2} \tag{3}$$

From the transient network settings and other recorded data, the energy level for each electron trapping state was calculated. Simply, the energy level was determined by using data gathered from separate temperature sweeps with the same test sample. When the DLTS experiment was cycled on the same sample with different emission rates, the peak temperature of the trapping state shifted. The peak temperature for each emission rate was recorded, and the energy level for each trapping state was calculated from the following equation:

$$E = - \frac{\ln(e_{R1}/e_{R2})\ K}{\left(\frac{1}{T_1} - \frac{1}{T_2}\right)} \tag{4}$$

(Appendix B)

where E is the energy level of the trapping state, e_{R1} is the emission rate for the first sweep, e_{R2} is the emission rate for the second sweep, T_1 is the peak temperature for the first sweep, T_2 is the peak temperature for the second sweep, and K is Boltzmann's constant.

Oscilloscope

A Tektronix type 7514 storage oscilloscope was used to observe the capacitance transient changes across the deple-

tion region of each test sample. A noticeable change in the transient curve was observed whenever a trapping level was detected (Fig. 16). This change was identified by a slight increase in the slope of the transient.

The forward conduction (current pulses) of several test samples was observed on the oscilloscope with a current probe connected to the sample circuit. The observed current pulses occurred with every injection pulse from the pulse generators. Thus, the current pulses had a 70 msec period also (Fig. 14).

The usual current-voltage characteristic of each test sample was observed and recorded by a Tektronics (Type 577) curve tracer oscilloscope. This observation was done both before and after the sample was irradiated and otherwise prepared for the DLTS experiment.

The curve tracer was used to observe the current-voltage (I-V) characteristics of a test sample from helium temperature to room temperature. At 4.2°K the oscilloscope showed almost zero current and voltage. As the sample was slowly heated to 300°K, a family of I-V curves were recorded (Fig. 17).

X-Y Recorder

A Varian F-81 X-Y recorder was used to display all plots of the electron trapping states. Inputs from the boxcar (Y-coordinate) and the sample's thermocouple (X-coordinate) were used to provide the trapping states spectroscopic displays (Fig. 13).

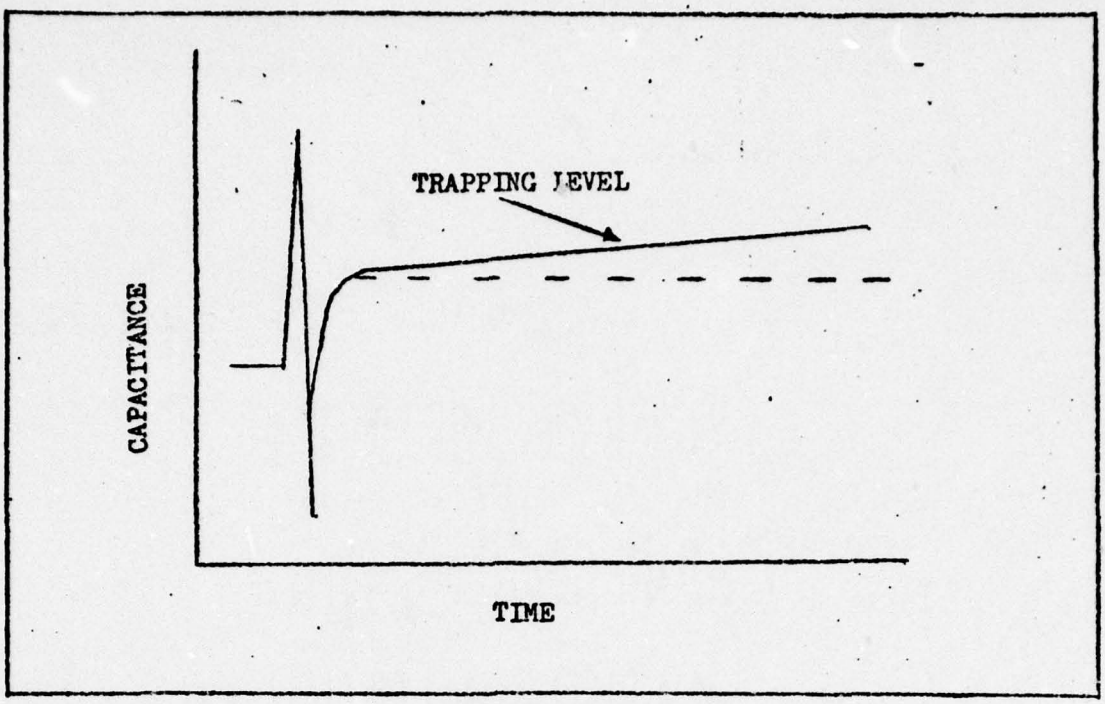

Fig. 16. Detection of Trapping Level.

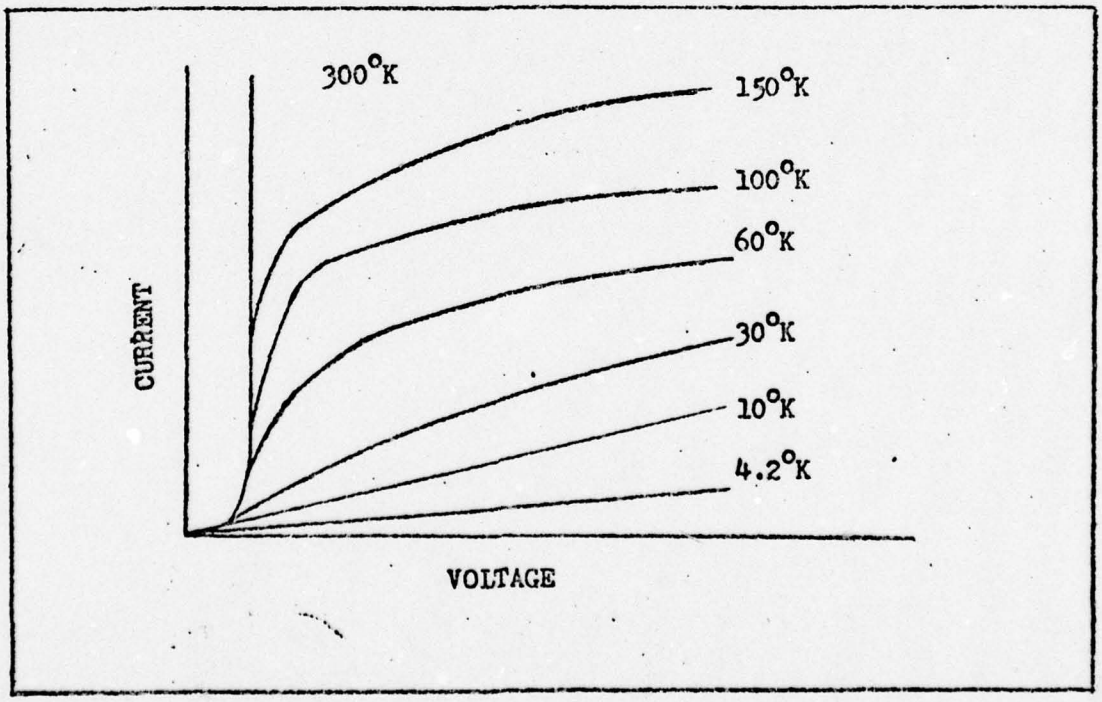

Fig. 17. Family of I-V Curves For R9-2-4 At Various Temperatures.

Profiler

An automatic doping profiler manufactured by Material Development Corporation was used to produce rapid and accurate information about the impurity distribution of each test sample. The profiler consists of a capacitance meter, a bias control, associated analog circuitry, and an x-y recorder. The equipment can be operated in two operational modes: the capacitance-voltage (C-V) mode and the concentration-depth (N-W) mode.

In the C-V mode a test sample is connected across the capacitance meter and the bias control is then used to sweep the sample from zero to approximately 10.0 volts. The resultant output (C-V curve) is plotted on the x-y recorder.

Concentration-depth information is derived from the C-V data automatically in the N-W mode. As the bias supply is swept, an analog signal proportional to the capacitance is made available to the capacitance meter. This dC/dV signal arises from the super-position of a small 1 K Hz signal on the direct current bias. At the output of the capacitance meter these signals are detected and plotted on the x-y recorder to give the desired N-W profiles.

IV. Experimental Results

The deep level trap spectroscopy experimental work was primarily performed on the field effect devices from wafer R9. This wafer was selected because its devices had approximately uniform characteristics. Measurements used to determine similar characteristics included current-voltage, capacitance-voltage, and concentration-depth profiles. Specifically, the FET devices labeled R9-1-4, R9-2-4, R9-6-4, R9-7-4, and R9-8-4 were tested (Fig. 5).

Test sample R9-1-4 was subjected to a series of electron dosages from 1 X $10^{14}cm^{-2}$ to 5 X $10^{15}cm^{-2}$ (Fig. 18-21). Increasing electron irradiation dosages greatly altered the sample's doping profile. It was observed that similar irradiation of the other FET devices from wafer R9 produced nearly identical profiles. Therefore, these irradiative doping profiles were representative of the other test samples as well. A plot of the capacitance versus voltage of test sample R9-2-4, both before and after electron irradiation, is shown in Fig. 22. Again this plot is representative of all the test samples.

The DLTS experiment was conducted on each test sample which had been irradiated at a specific electron dosage. Each specific dosage induced electron trapping states which were detected by the transient capacitance network. The plots recorded for the various test samples are shown in

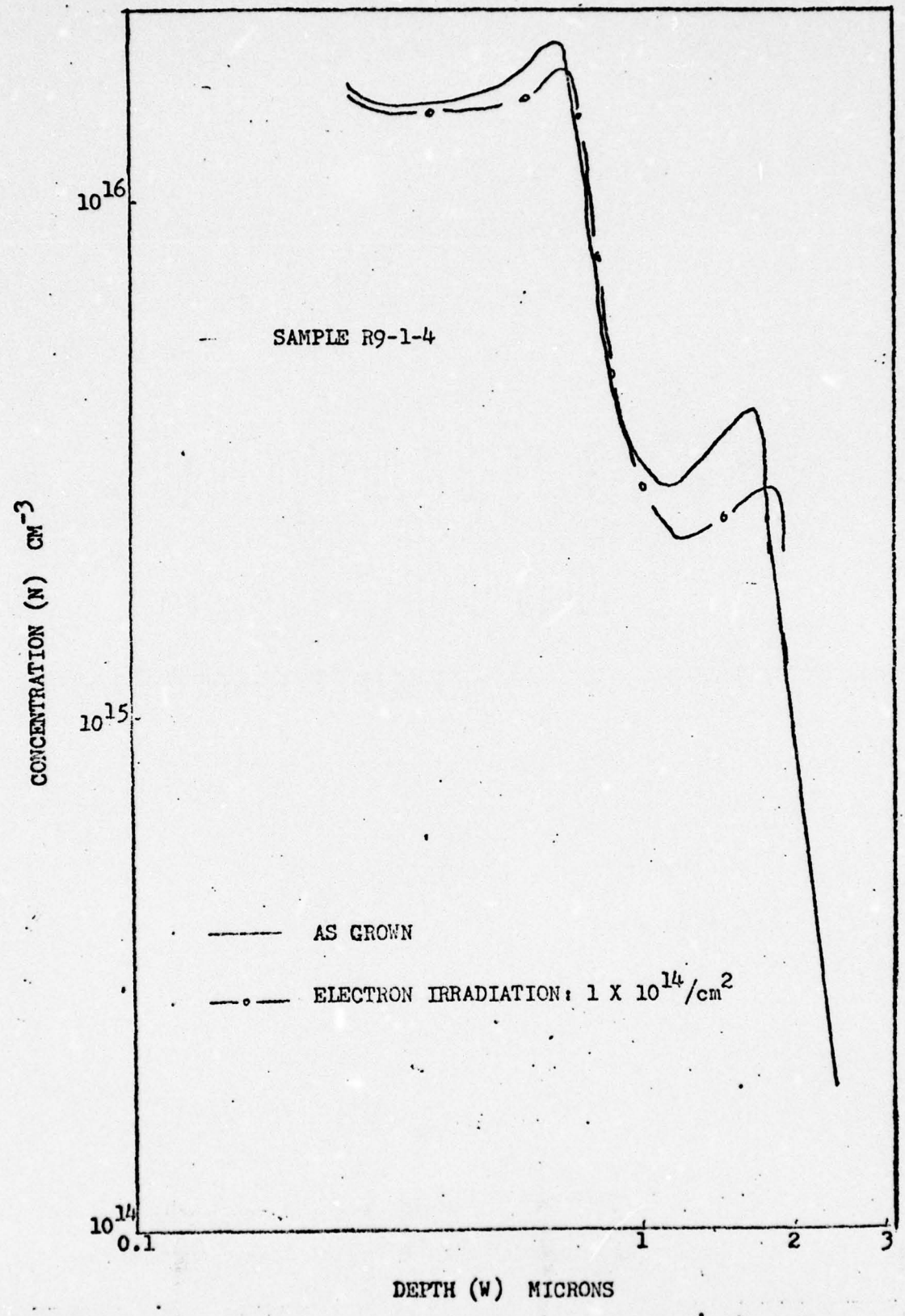

Fig. 18. Test Samples Doping Profile: 1 X $10^{14}/cm^2$

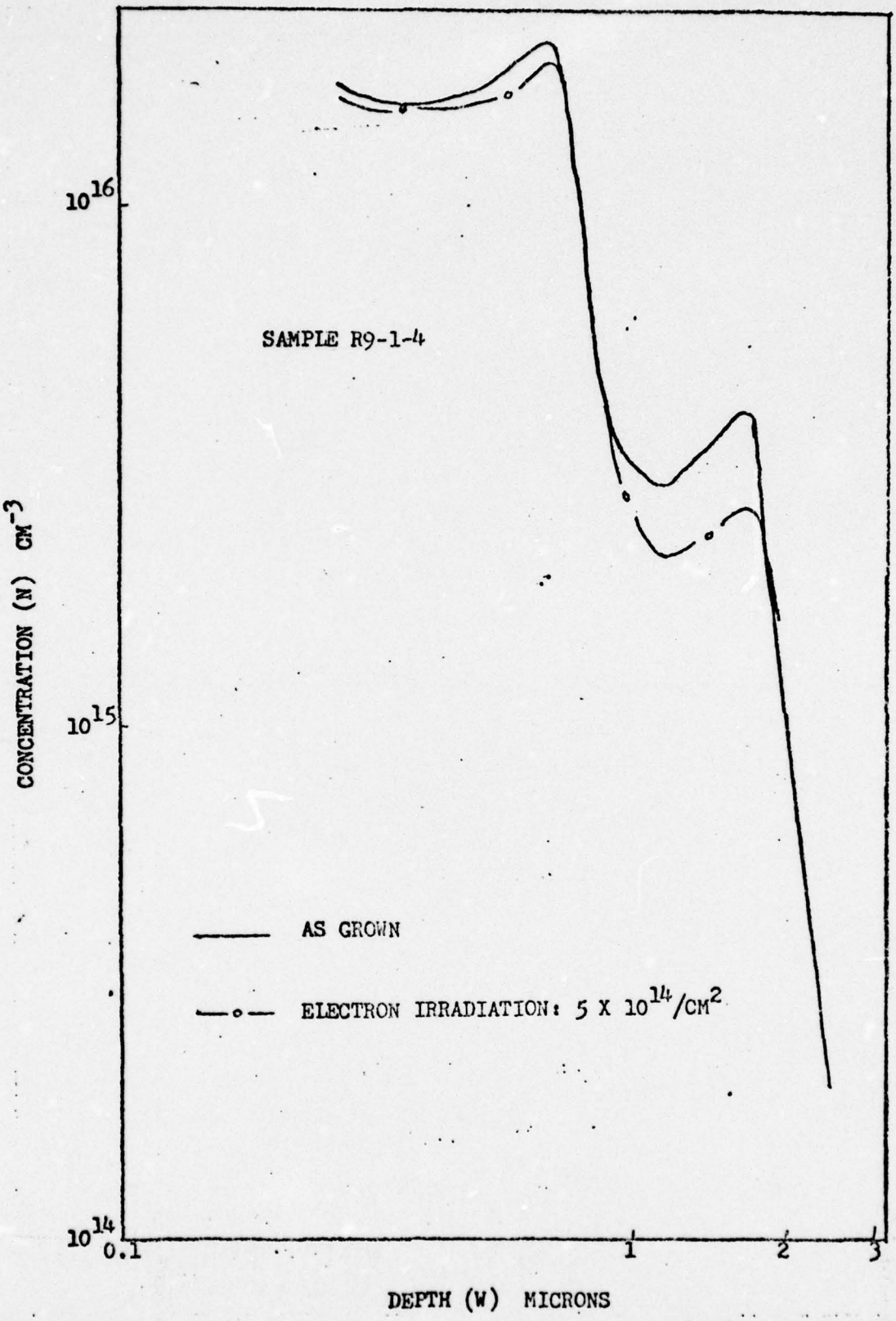

Fig. 19. Test Samples Doping Profile: 5 X $10^{14}/cm^2$

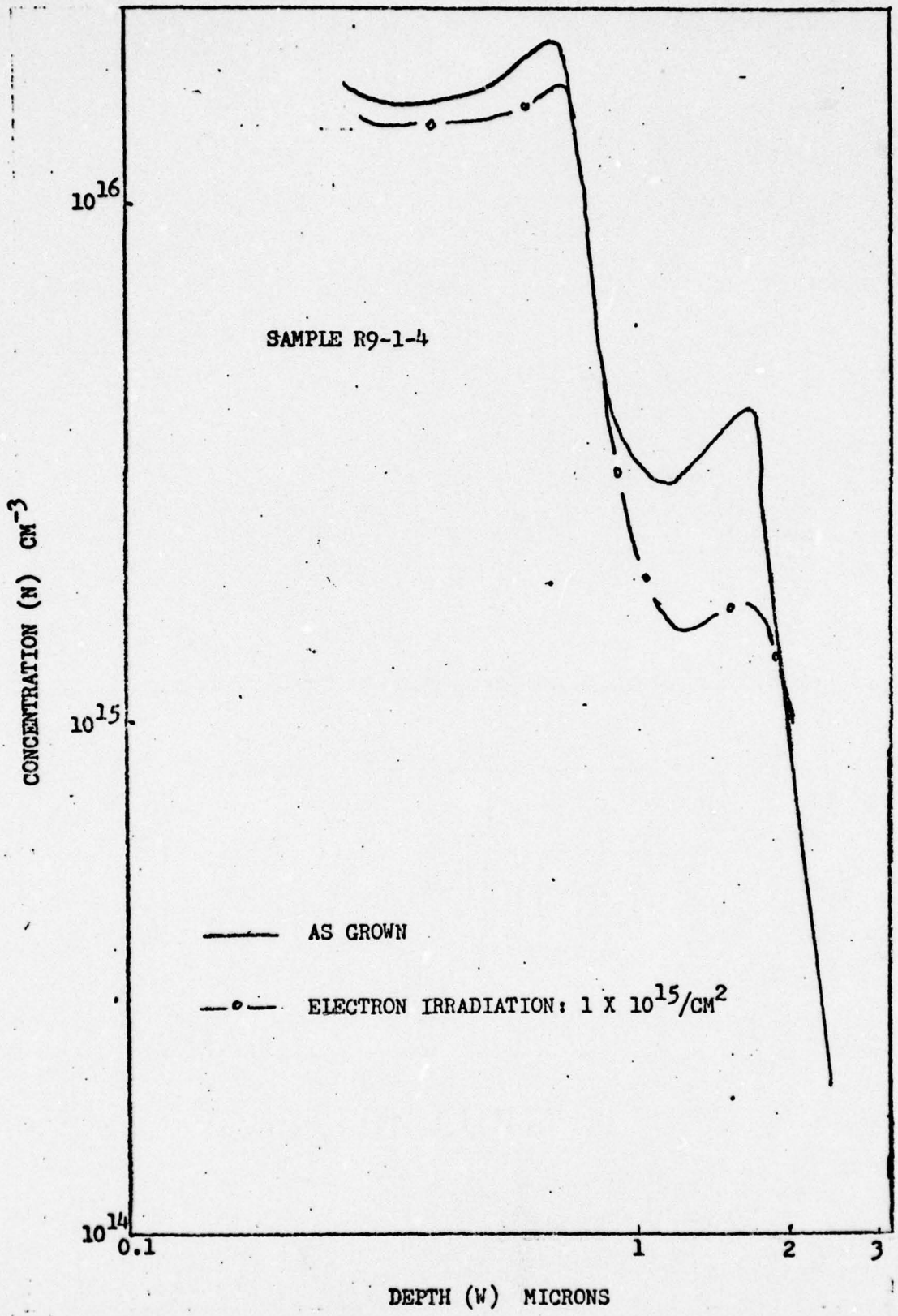

Fig. 20. Test Samples Doping Profile: 1 X $10^{15}/cm^2$

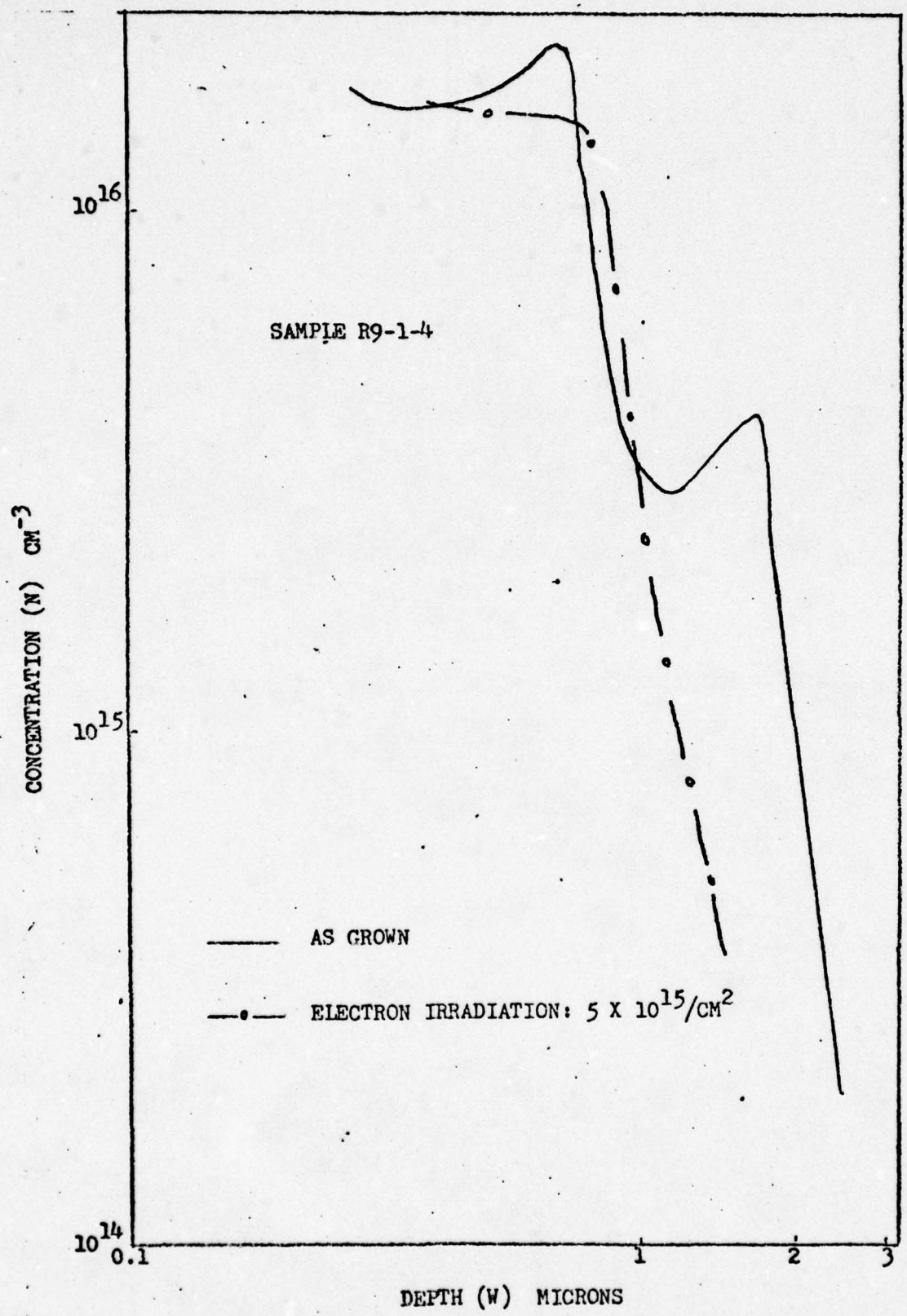

Fig. 21. Test Samples Doping Profile: 5 X $10^{15}/cm^2$

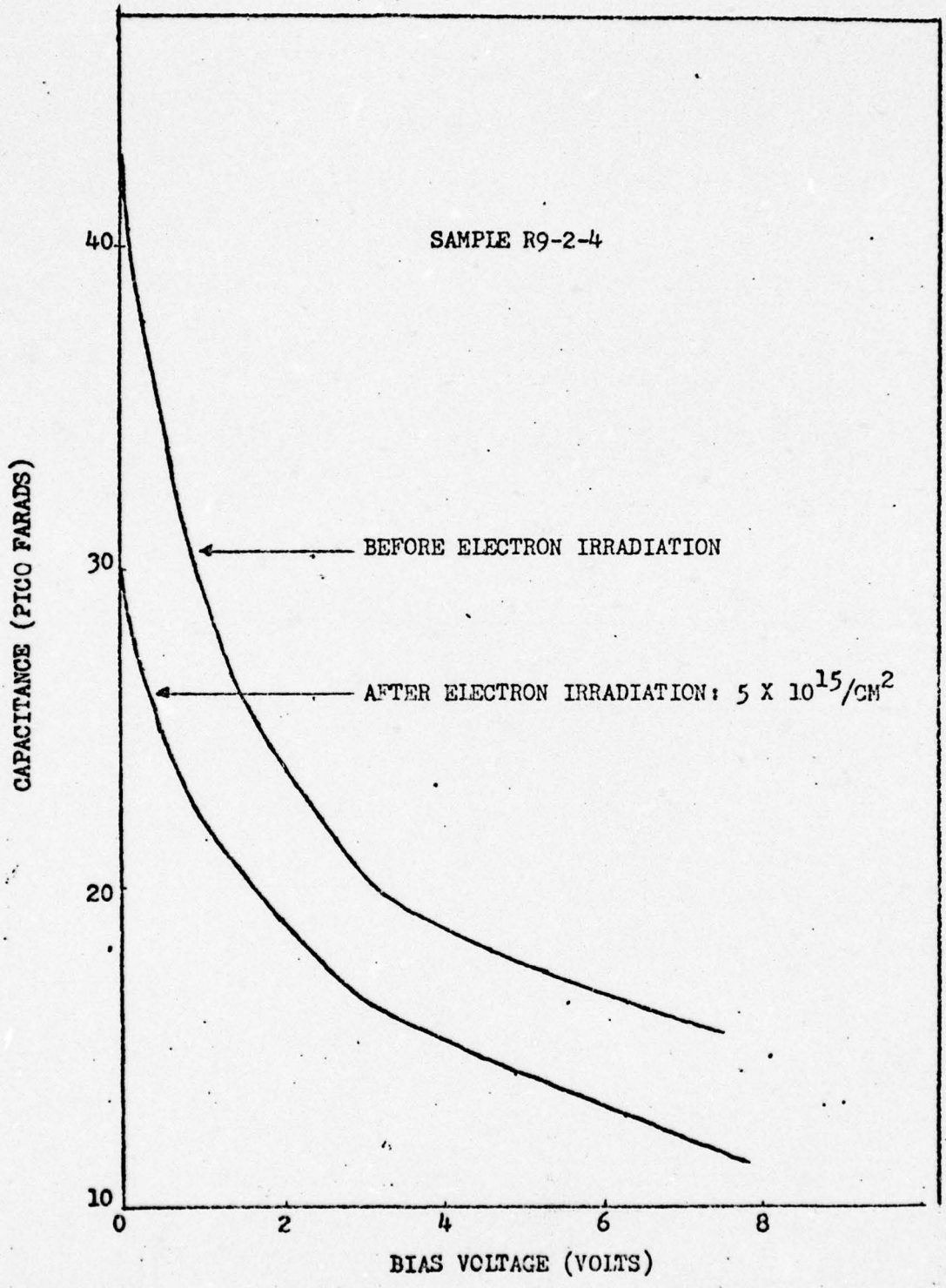

Fig. 22. Test Samples C-V Characteristics.

Figs. 23-29. The electron dosages for successive test samples were increased in the following manner: R9-8-4: $1 \times 10^{14}/cm^2$, R9-7-4: $5 \times 10^{14}/cm^2$, R9-6-4: $1 \times 10^{15}/cm^2$, and R9-2-4: $5 \times 10^{15}/cm^2$. Table I shows the peak temperatures of the trapped states for three of the irradiated test samples. The various bias voltages used for each thermal scan are also shown in this table.

The characterization of the induced trapping states was done by analyzing test sample R9-2-4. This sample, which was subjected to the largest electron irradiation damage, was cycled through the DLTS experiment at various emission rates. Table II shows the peak temperatures observed for each emission rate. The characterization of the electron-induced traps was done by calculating the energy levels at which the traps occurred and by calculating the trap concentration of each level.

Specifically, the peak temperatures observed along with their corresponding emission rates were used to calculate the energy level of three trapping states. Figure 30 shows a composite summary of these peak temperatures at four distinct emission rates. The spectroscopic curves displayed represent selective data extracted from Table II. A semi-logarithmic plot of emission rate versus the reciprocal of temperature for the peak temperatures under column T1 of Table II is shown in Fig. 31. Similarly, Figs. 32 and 33 show plots of the data under column T3 and T4 respectively. The peak temperatures shown in Fig. 33, however, represent

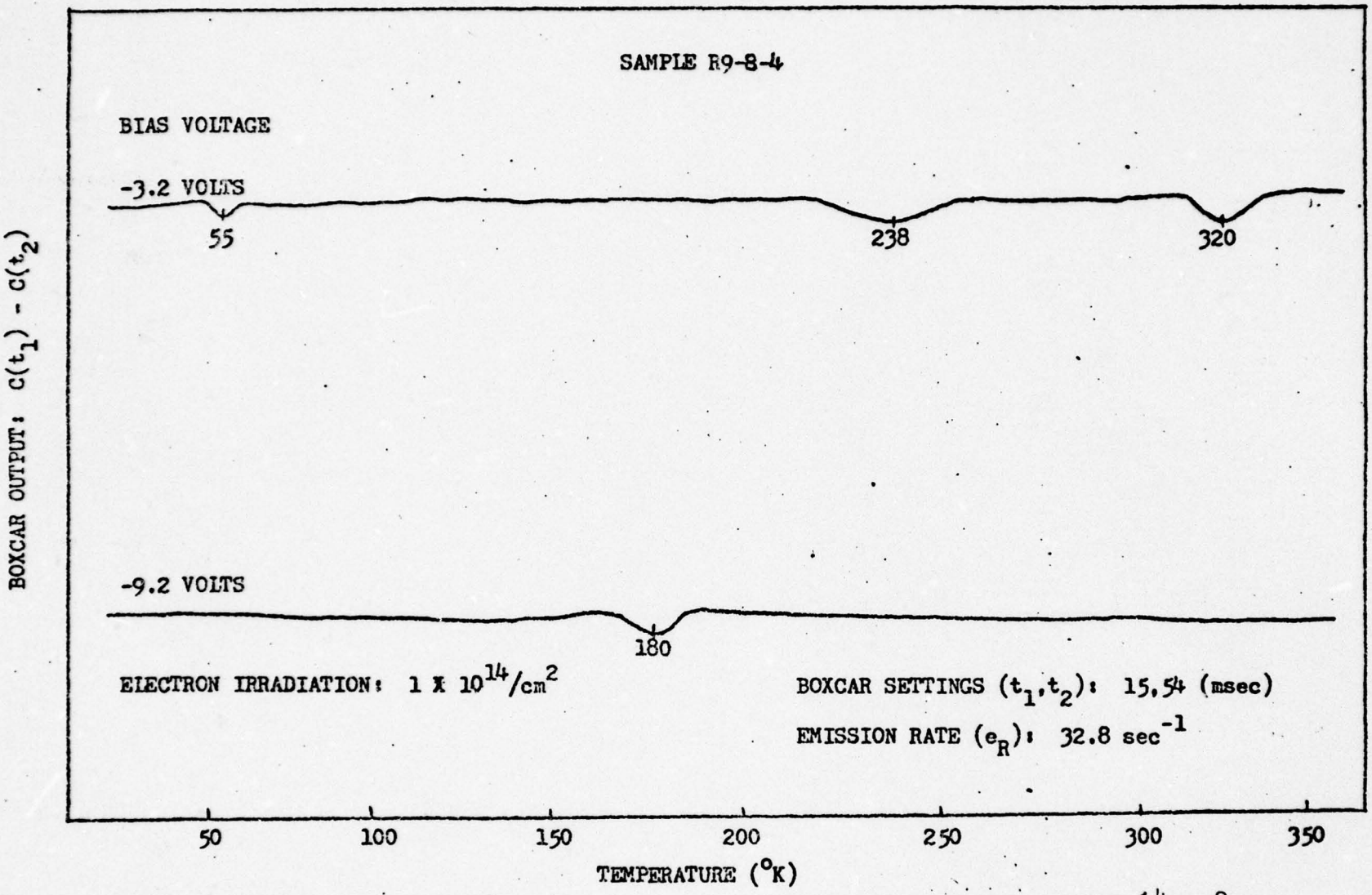

Fig. 23. Electron Traps From Sample R9-8-4 Irradiated at 1 X $10^{14}/cm^2$.

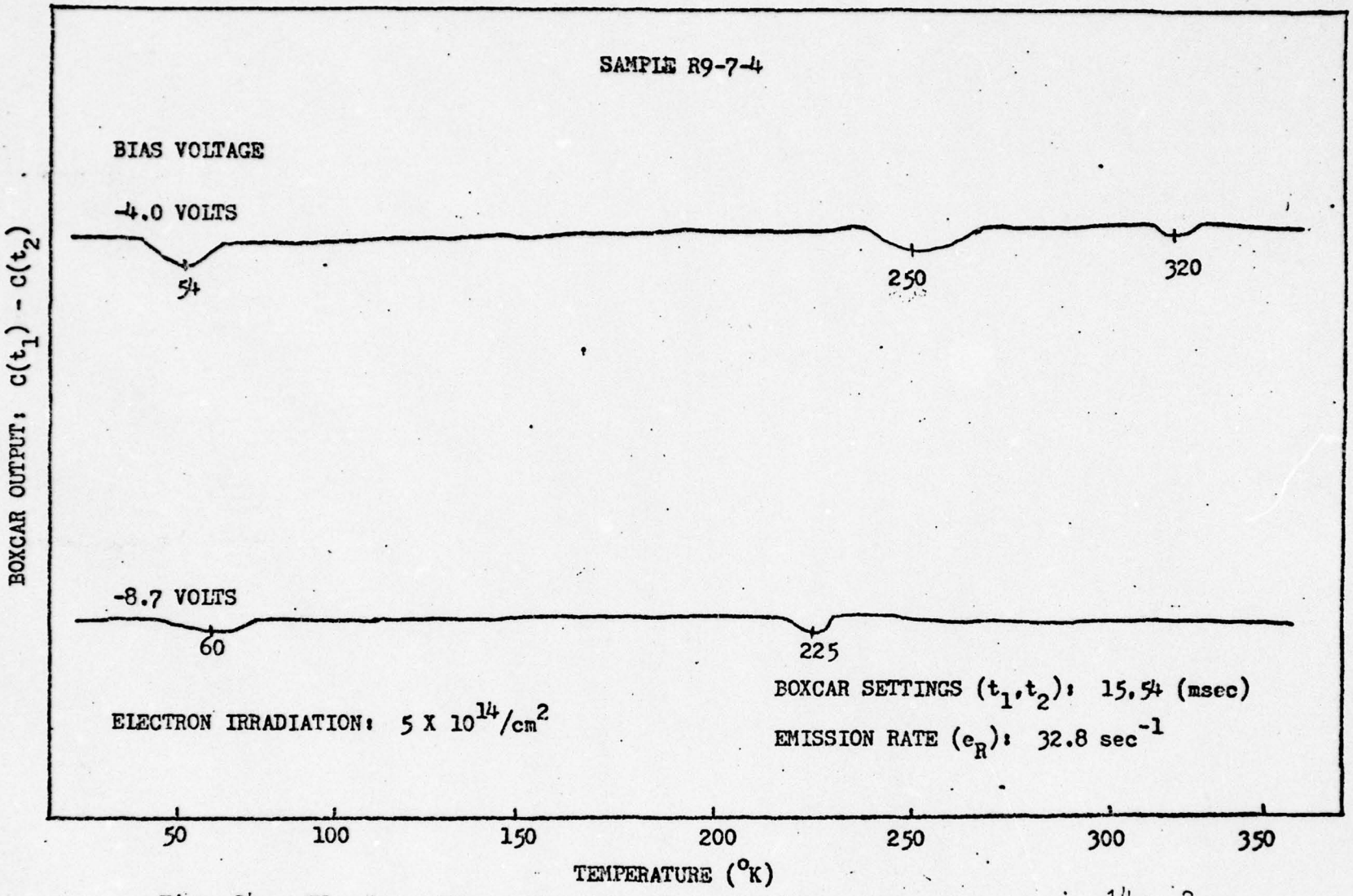

Fig. 24. Electron Traps From Sample R9-7-4 Irradiated at 5 X $10^{14}/cm^2$.

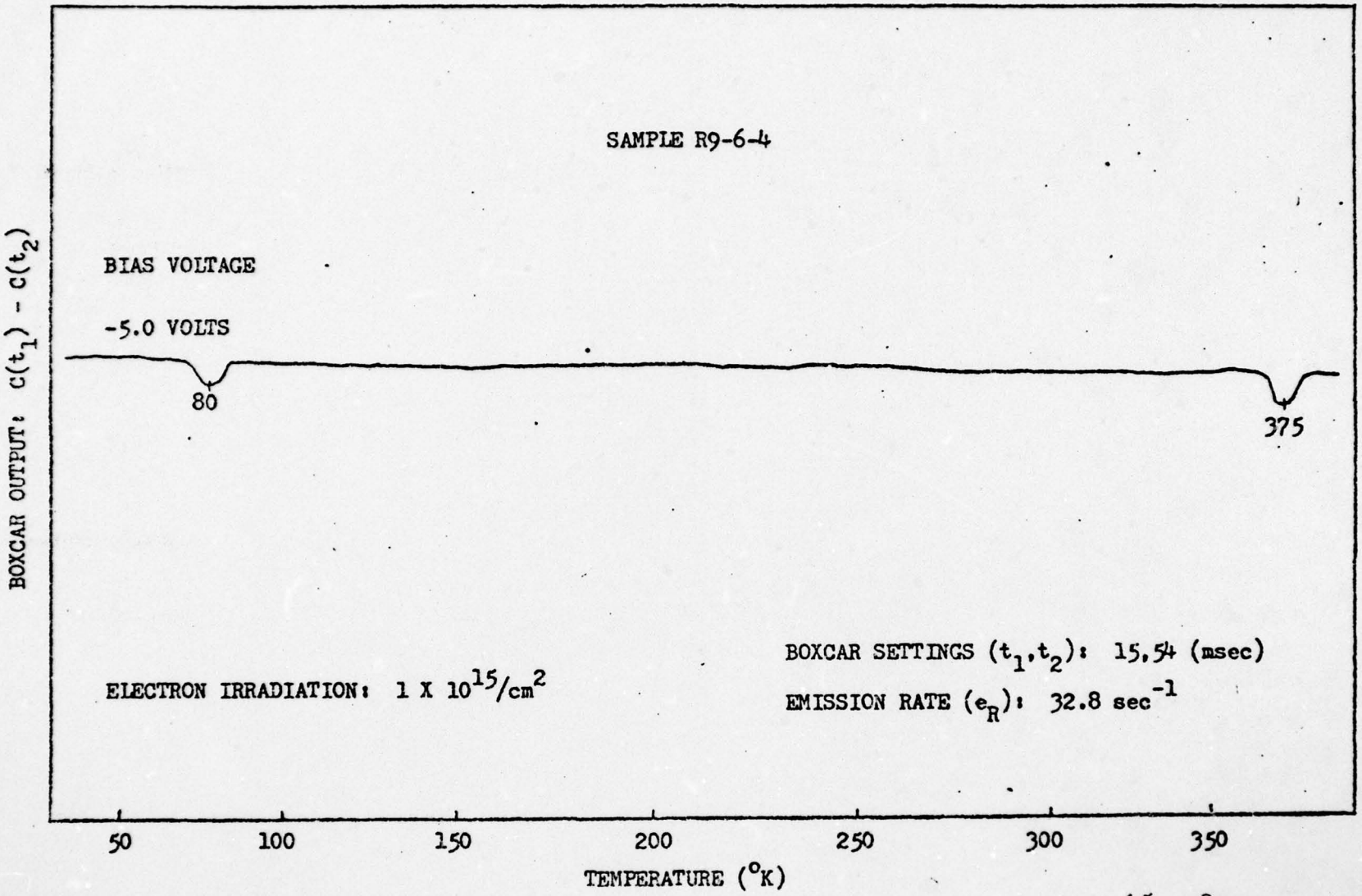

Fig. 25. Electron Traps From Sample R9-6-4 Irradiated at 1 X $10^{15}/cm^2$.

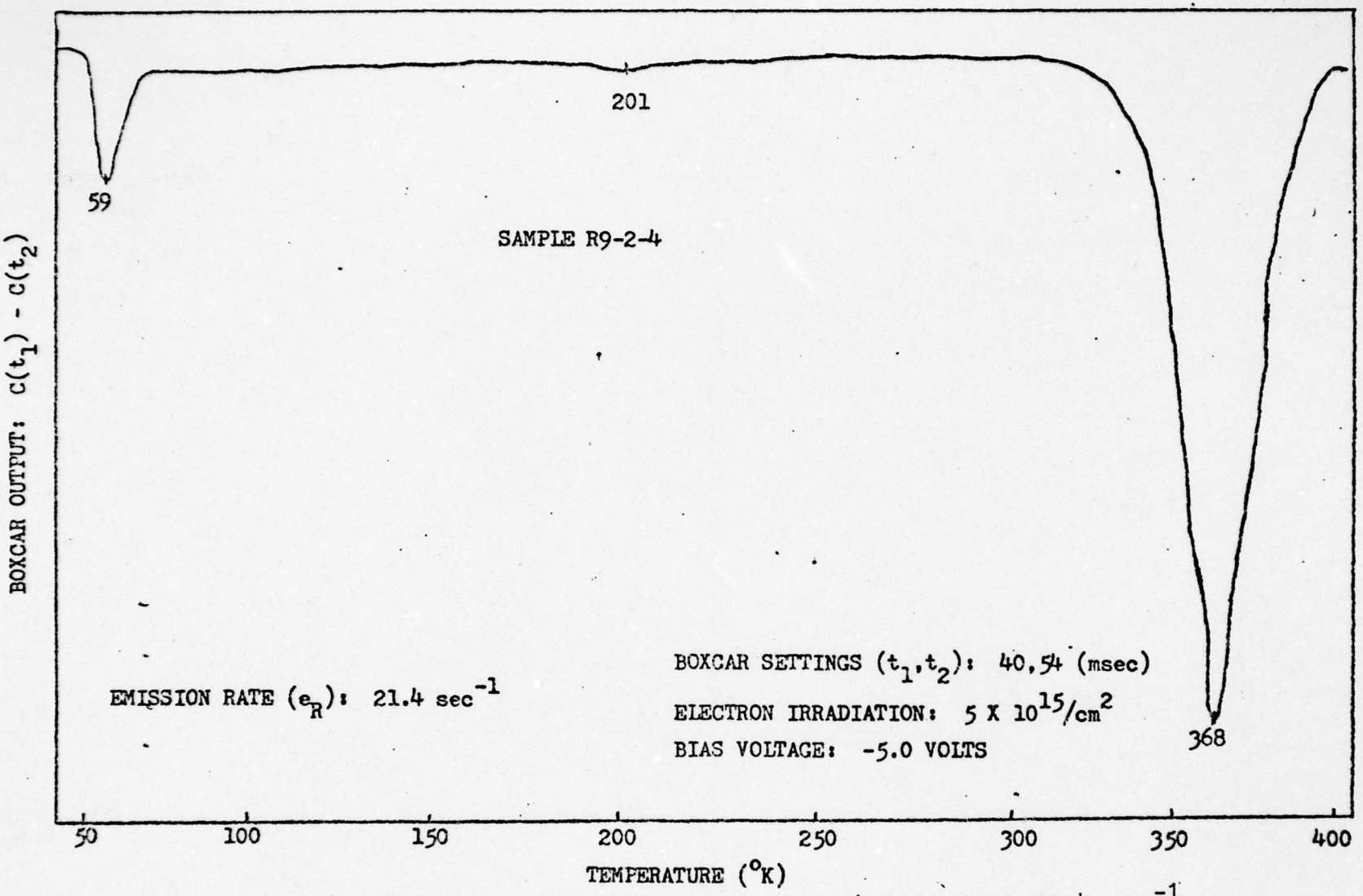

Fig. 26. Electron Traps From Sample R9-2-4 Cycled at 21.4 sec^{-1}.

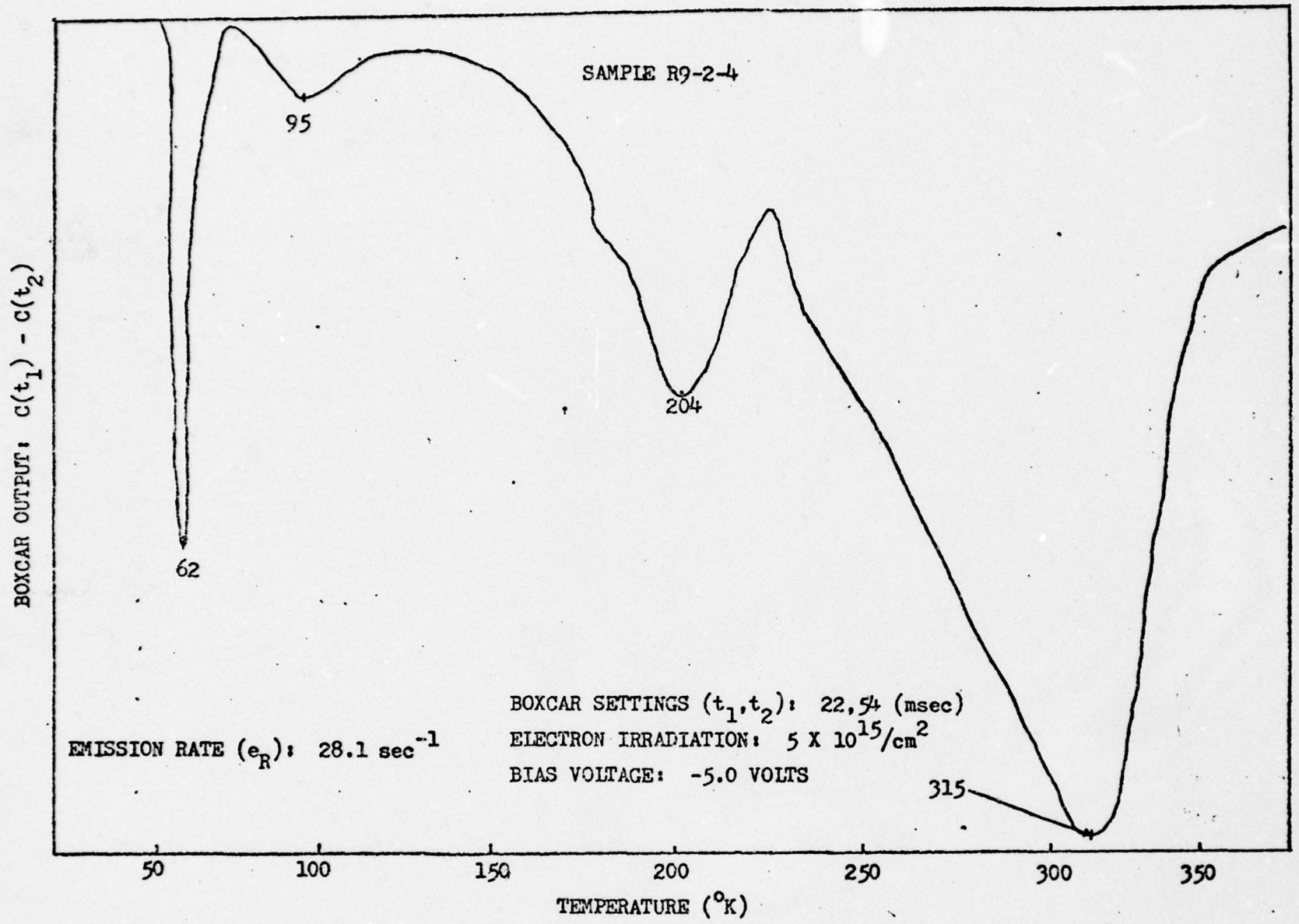

Fig. 27. Electron Traps From Sample R9-2-4 Cycled at 28.1 sec^{-1}.

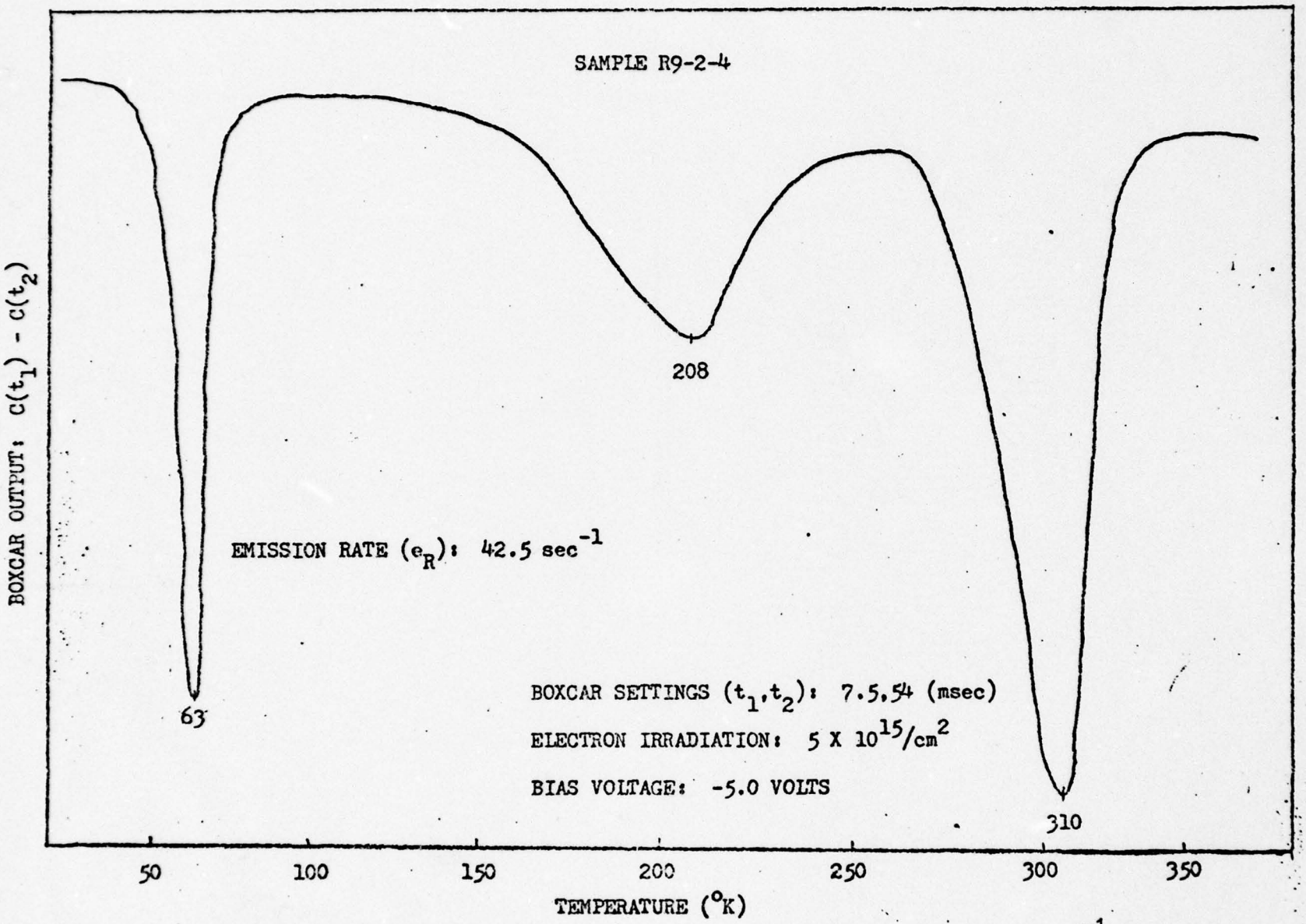

Fig. 28. Electron Traps From Sample R9-2-4 Cycled at 42.5 sec^{-1}.

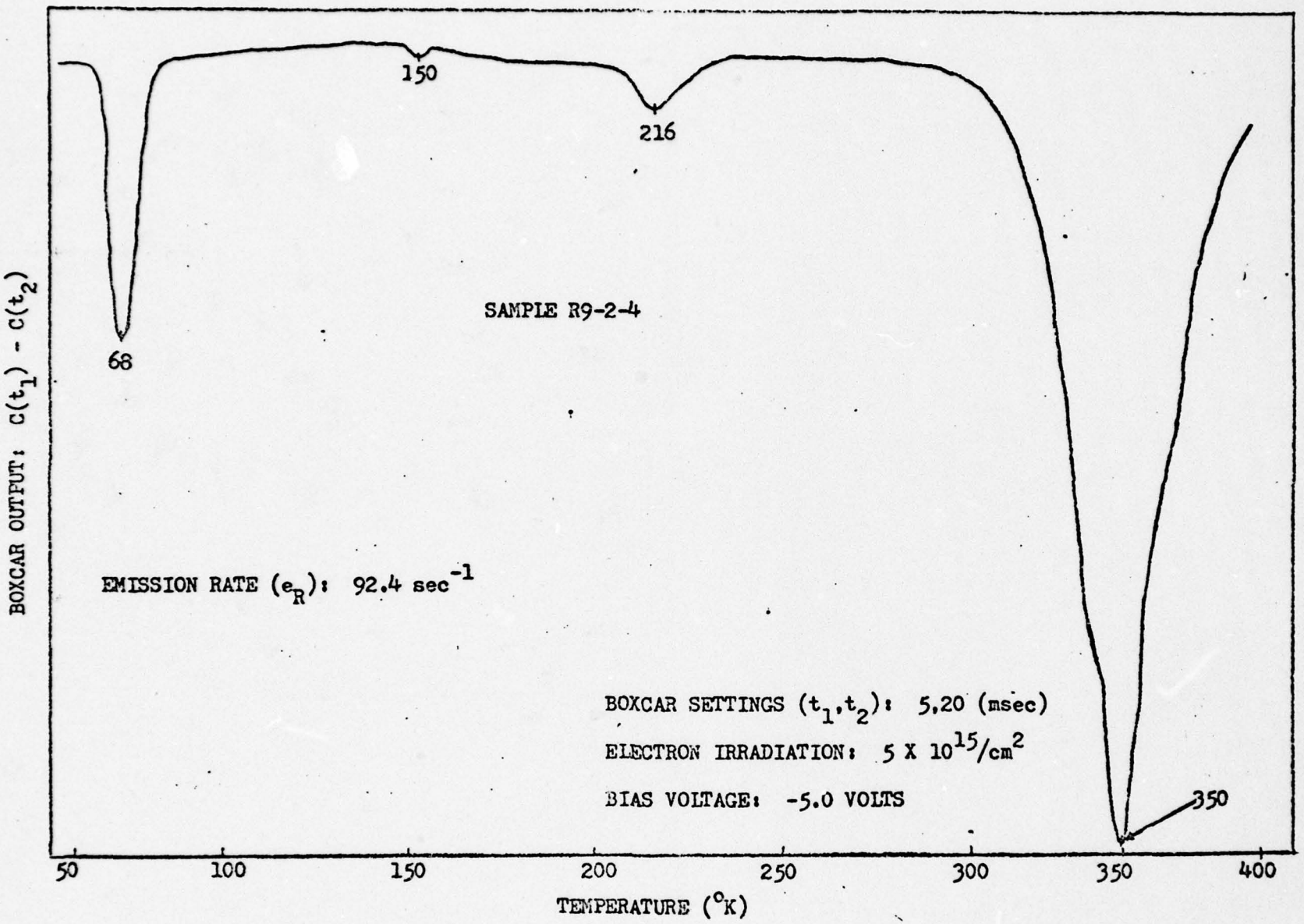

Fig. 29. Electron Traps From Sample R9-2-4 Cycled at 92.4 sec^{-1}.

Table I
Trapping State Peak Temperatures For Three Test Samples

BOXCAR SETTINGS: (15, 54) msec

EMISSION RATE: 32.8 sec^{-1}

TEST SAMPLE	BIAS VOLTAGE (VOLTS)	PEAK TEMPERATURES ($^{\circ}K$)				
		T_1	T_2	T_3	T_4	T_5
R9-8-4 ELECTRON DOSE: $1 \times 10^{14} cm^{-2}$	1.1	45	-	-	360	-
	2.3	45	-	238	360	-
	3.2	55		238	320	
	9.6	-	-	180	-	-
R9-7-4 ELECTRON DOSE: $5 \times 10^{14} cm^{-2}$	1.6	60	-	200	-	-
	2.5	60	-	-	-	-
	3.5	59	-	-	-	-
	4.0	54	-	250	320	-
	5.0	59	-	-	-	-
	8.7	60	-	225	-	-
R9-8-4 ELECTRON DOSE: $1 \times 10^{15} cm^{-2}$	5.0	80	-	-	375	-

Table II
Trapping State Peak Temperatures For Sample R9-2-4

BIAS VOLTAGE: -5.0 VOLTS

SAMPLE R9-2-4 ELECTRON DOSAGE: 5 X $10^{15}/cm^{-2}$

EMISSION RATE $e_R = \frac{\ln(t_1/t_2)}{t_1 - t_2}$ (SEC^{-1})	BOXCAR SETTINGS t_1, t_2 (MSEC)	TIME CONSTANT $\frac{1}{e_R}$ (MSEC)	PEAK TEMPERATURES (°K)				
			T_1	T_2	T_3	T_4	T_5
21.1	45, 50	47.4	58	-	198	325	
21.4	40, 54	46.7	59	-	201	368	452
			-	-	-	312*	464*
28.1	22, 54	35.6	62	95	204	315	464
42.5	7.5, 54	23.5	64	125	210	349	443
			63	-	208	310	-
			65	-	-	354	-
			64	-	196	-	-
			-	-	-	318*	460*
61.6	7.5, 30	16.2	-	-	-	319*	-
			-	-	-	338*	-
92.4	5, 20	10.8	67		216	384	-
			68	150	216	350	-
			-	-	-	325*	-

*High Temperature Sweeps

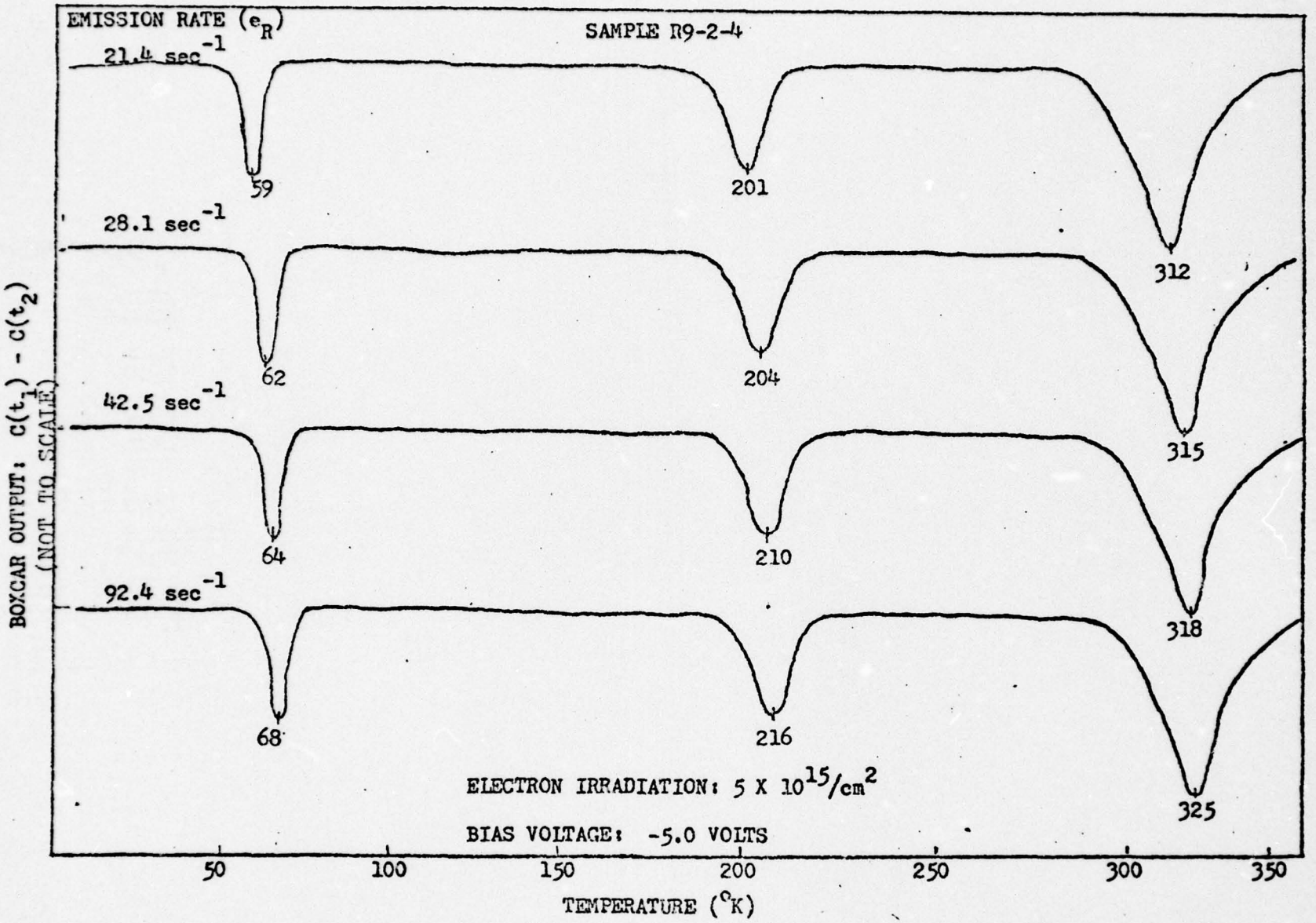

Fig. 30. Composite Summary of Peak Temperatures at Various Emission Rates.

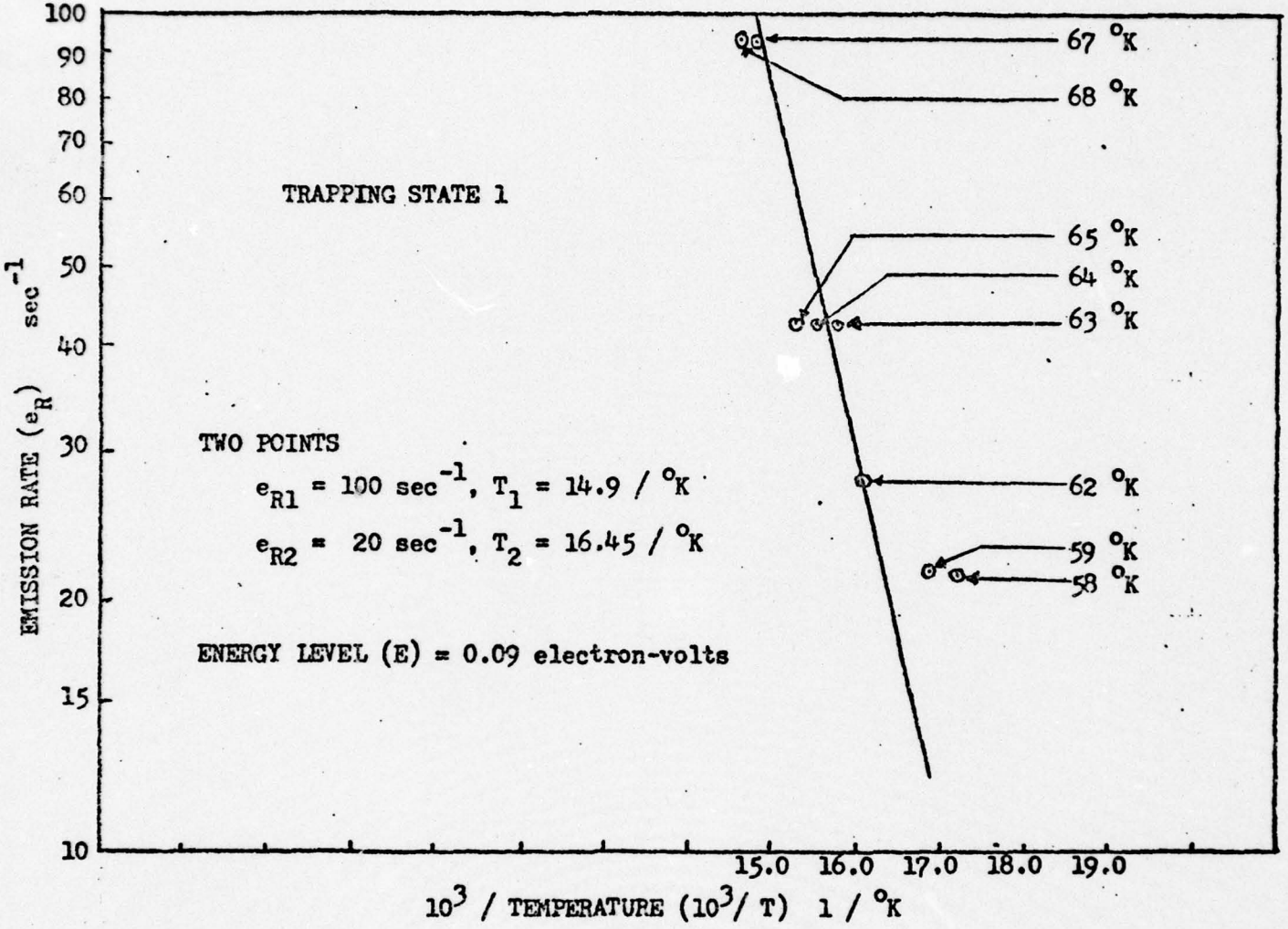

Fig. 31. E_R vs $10^3/T$ for Trapping State 1.

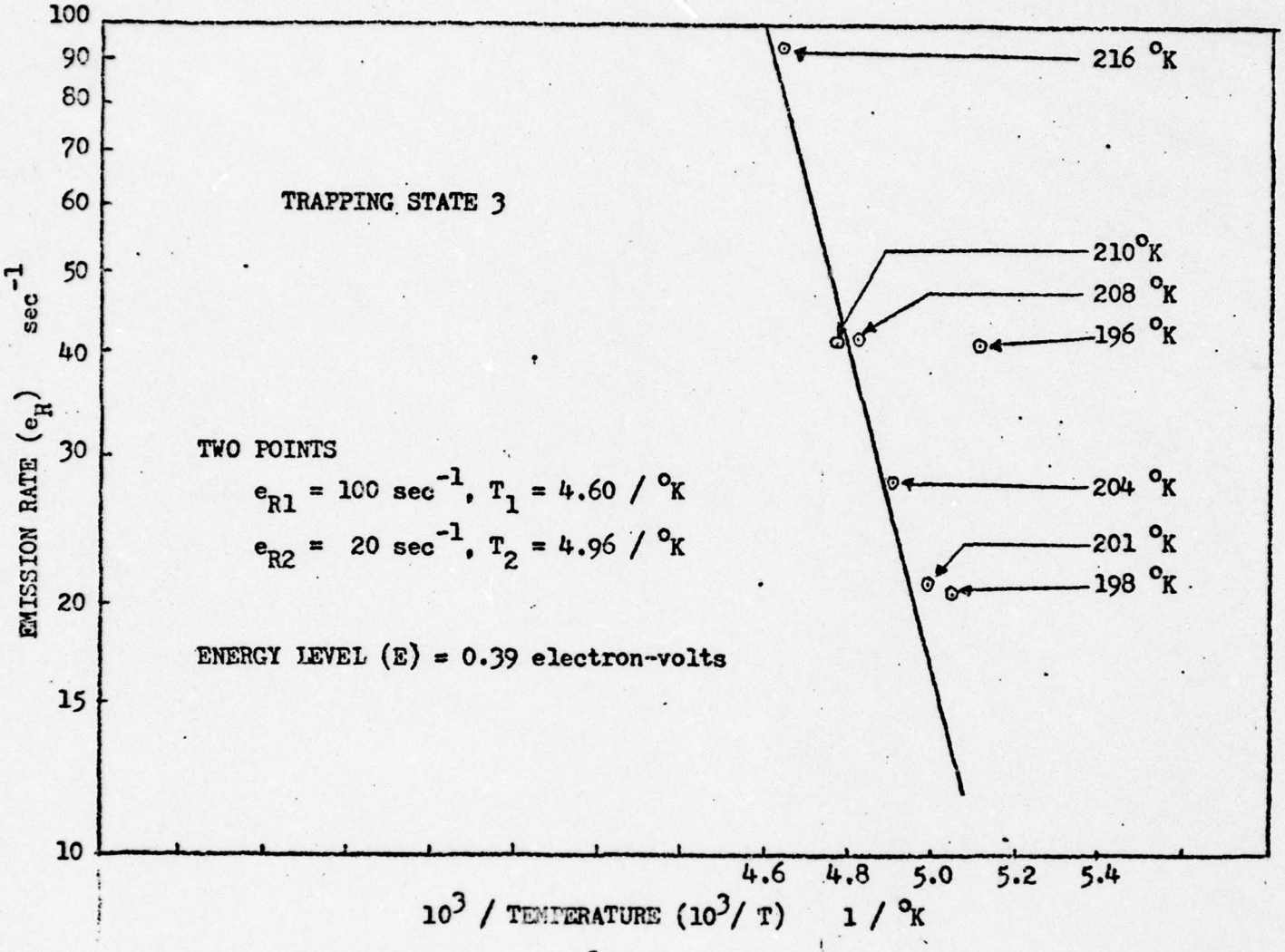

Fig. 32. E_R vs $10^3/T$ for Trapping State 3.

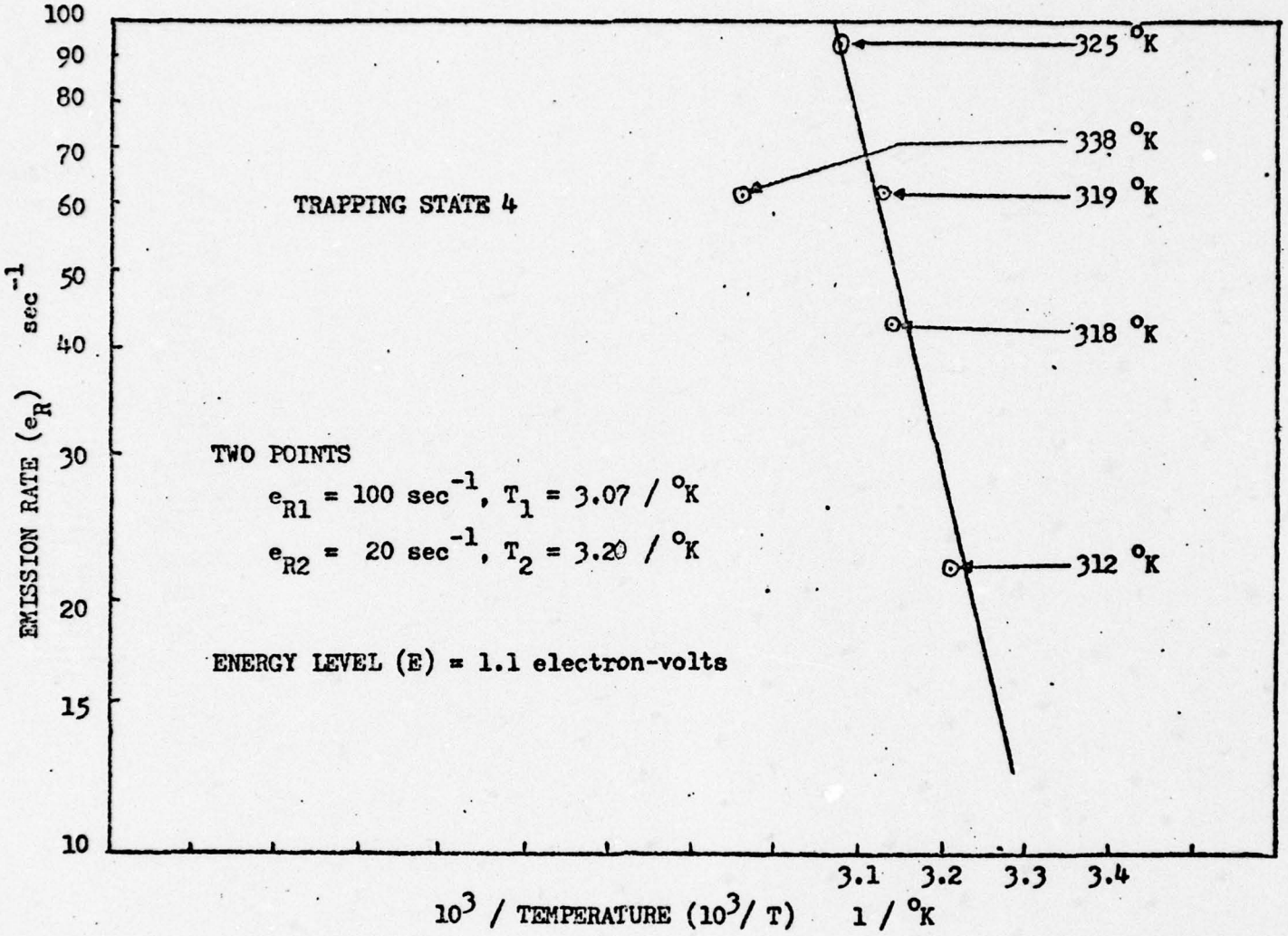

Fig. 33. E_R vs $10^3/T$ for Trapping State 4.

only the high temperature DLTS sweeps. Two points (e_{R1}:T1 and e_{R2}:T2) from the straight line plotted in these figures were used in Eq. 4 to calculate the energy level of each trapping state. The result of this calculation is shown on each figure.

The trap concentration was calculated using the empirical relationship cited in reference 6. Table III shows the results computed for each trapping state. The sensitivity of the system was determined by measuring ΔC and C at several peaks. It was determined that a peak one division high on the recorder could be clearly separated from the noise and this would represent a $\Delta C/C$ of 10^{-3}.

Table III
Trap Concentration Calculation of the Trapping States

SAMPLE R9-2-4

ELECTRON IRRADIATION: $5 \times 10^{15} cm^{-2}$

$N_T = 3(\frac{\Delta C}{C})N$, $N = 10^{16} cm^{-3}$

TRAPPING STATE	$\frac{\Delta C}{C}$/DIVISION	NO. OF DIVISIONS	TRAP CONCENTRATION (N_T) CM^{-3}
1	10^{-3}	5	1.5×10^{14}
3	10^{-3}	140	4.2×10^{15}
4	10^{-3}	10	3.0×10^{14}

V. Conclusions and Recommendations

Since the purpose of this study was to characterize deep traps in epitaxial gallium arsenide sample by DLTS, the conclusions which have been drawn address the characterization process and the insights gained regarding trap occurrence and behavior.

Errors Involved

There were several opportunities for errors to affect the experimental data. Errors in the peak temperatures recorded are possible since the thermocouple was not mounted exactly on the sample, but on the coldfinger, nearly two inches above the sample. At the beginning of the DLTS run near absolute zero (4.2°K), the liquid He was shut off and the sample was permitted to warm primarily by radiation. Hence, the sample would be warmer than the thermocouple. This is believed to be a major factor in the discrepancy in the measured activation energy of the first trap compared to previously published reports (Refs. 3, 7, 8). Above 70°K the heater was used for warming. Hence, at higher temperatures, especially above room temperature, the thermocouple temperature would be higher than the sample temperature. In comparing the peak temperatures on full (4.2°K to 450°K) temperature sweeps with sweeps from 300°K to 450°K, differences of 50°K were observed.

Another source of possible error was in the measurement of the capacitance. A noticeable capacitance discrepancy for several samples was detected while monitoring the capacitance meter as a function of bias voltage. These inaccurate capacitance readings were attributed to a blown fuse in the meter. Errors of this nature were difficult to detect since the capacitance meter did not indicate blown fuses. However, it was concluded that these errors were infrequent during the DLTS experiment.

There were several data points which were inconsistent with the rest of the data. Some of these anomalies are unexplained. Other factors such as distortion of the transient decay by pulses transmitted through the capacitance meter, small oscillations of the quiescent valve of the capacitance, and noise were noted during some of the temperature sweeps. All of these factors had to be considered when selecting an appropriate slope to calculate the activation energy.

Summary and Conclusions

Trapping states in epitaxial gallium arsenide induced by MeV electron irradiation were successfully measured and characterized by the DLTS technique. Several n-type epitaxial GaAs samples with a buffer layer were irradiated at room temperature at doses ranging from $10^{14}cm^{-2}$ to $10^{16}cm^{-2}$. Noticeable changes in the sample's doping profile were observed from the series of electron dosages. In particular, the depth of the buffer layer was varied from approximately

2.5 microns to 1.5 microns at a concentration of nearly $10^{15}cm^{-3}$ (Figs. 18-21). In addition, a significant reduction in the amplitude of the C-V plot of the sample was apparent after irradiation (Fig. 22). It was concluded that the electron dosages induced the deep traps (material defects) since the DLTS spectrum before irradiation showed no electron traps.

The DLTS experiment measured a gradual increase in the concentration of the induced trapping states with increased radiation dose. The concentration of the trapping states was directly proportional to the magnitude of the peaks observed. Samples irradiated from $10^{14}cm^{-2}$ to $10^{15}cm^{-2}$ had small peaks (Figs. 23-25). However, samples irradiated at $5 \times 10^{15}cm^{-2}$ had induced trapping states with large peaks (Figs. 26-29). The calculation of the trap concentrations in Table III supports this observation. In addition, a summation of the trap concentrations for the three trapping states in Table III totals $4.65 \times 10^{15}cm^{-3}$. This figure is very close to the electron irradiation dosage of $5 \times 10^{15}cm^{-2}$ for sample R9-2-4. Thus, the material defects introduced by electron damage nearly equaled the sum of the trap concentrations for a given sample, suggesting that under these conditions impinging electrons have a high probability of generating trapping states. The activation energy computed for the trapping states compares favorably with the results obtained from other publications (Refs. 3, 7, 8). The data suggest a strong correlation with trapping states occurring

at peak temperatures near 65°K, 210°K, and 320°K. The activation energies computed for these peak temperatures were 0.09 eV, 0.39 eV, and 1.1 eV.

The DLTS technique is well suited to studies of this kind since it is possible to independently vary both the average charge state and the electron-hole recombination rate at a particular defect. The charge state can be varied by placing the observed traps either in the depletion region (reverse bias) or in neutral material (zero bias). Electron-hole recombination changes are present under forward bias (Ref. 7:489).

Recommendations

Recommendations are divided into two categories: recommendations for modifications to the experimental equipment and areas for further study. Specific recommendations are listed below:

1. The heli-tran cold finger should be modified to allow the thermocouple to be mounted closer to the test sample. This would reduce errors in the temperature measurements.
2. The process used to mount a test sample into the vacuum shroud is very cumbersome. An alternative method should be devised to facilitate such mounting.
3. The high vacuum equipment should be replaced. At present, the equipment takes too long to obtain the necessary vacuum for liquid helium transfer.

4. An indicating mechanism for blown fuses should be installed on the capacitance meter. This would reduce errors in the capacitance measurements.
5. A further study should be made to relate the electron traps to the overall design, manufacture, performance, and reliability of electron devices. Perhaps, a comprehensive comparison of several different device fabrication techniques should be made.
6. The electron traps should be further characterized in terms of defect identification. The identification would specify the appropriate chemical impurity or lattice imperfection of the trapped states. Perhaps, a comparison with several other techniques such as photocapacitance and Hall resistivity measurements would provide a correlation for analysis.

Bibliography

1. Cho, A. Y. "GaAs IMPATT Diodes Prepared by Molecular Beam Epitaxy." Applied Physics Letters, 25:224-226 (August 1974).

2. Eisen, F. H., et. al., Investigation of Technological Problems in GaAs. RADC TR 76-342. Rockwell International, California: Science Center, August 1976.

3. Kimerling, L. C. "New Developments in Defect Studies in Semiconductors." IEEE Transactions on Nuclear Science, 23:1497-1505 (December 1976).

4. Lang, D. V. "Fast Capacitance Transient Apparatus: Application to Zn O and O Centers in GaP p-n Junctions." Journal of Applied Physics, 45:3014-3021 (July 1974).

5. -----. "Deep-Level Transient Spectroscopy: A New Method to Characterize Traps in Semiconductors." Journal of Applied Physics, 45:3023-3032 (July 1974).

6. Lang, D. V. and A. Y. Cho. "Study of Electron Traps in n-GaAs Grown by Molecular Beam Epitaxy." Journal of Applied Physics, 47:2558-2564 (June 1976).

7. Lang, D. V. and L. C. Kimerling. "Observation of Recombination-Enhanced Defect Reactions in Semiconductors." Physical Review Letters, 33:489-492 (August 1974).

8. -----. "A New Technique for Defect Spectroscopy in Semiconductors: Application to 1 MeV Electron-Irradiated n-GaAs." Institute of Physics and Physical Society, Conference Series No. 3., 1975.

9. Lang, D. V., and R. A. Logan. "A Study of Deep Levels in GaAs by Capacitance Spectroscopy." Journal of the Electronic Materials, 4:1053-1066 (March 1975).

10. -----. "Deep Level Distributions near p-n Junctions in LPE GaAs." Journal of Applied Physics, 47:1533-1537 (April 1976).

11. Mircea, A. and A. Mitonneau. "A Study of Electron Traps in Vapor-Phase Epitaxial GaAs." Applied Physics, 8:15-21 (September 1975).

12. Okumura, T. and T. Ikoma. "New Method to Determine the Photoionization Threshold Energy of a Deep Level from Photocapacitance." Applied Physics Letters, 25: 572-574 (November 1974).

13. Schott, J. T., et. al., Transient Capacitance Measurement of Deep Defect Levels in GaAs and Si. AFCRL TR 76-0024. Hanscom Air Force Base, Massachusetts: Air Force Cambridge Research Laboratories, January 1976.

14. Wada, O., and S. Yanagisawa. "Determination of Deep Electron Traps in GaAs by Time-Resolved Capacitance Measurement." Applied Physics, 13:5-13 (March 1977).

Appendix A

Theory of DLTS

In order to explain DLTS, an understanding of the more basic problem of capacitance transients is necessary. The use of capacitance transients for trap studies in semiconductors is well known. This technique is used to obtain information about an impurity level in the depletion region of a Schottky barrier or p-n junction. This is done by observing the capacitance transient associated with the return to thermal equilibrium of the occupation of the level following an initial nonequilibrium condition. The activation energy for the level can be obtained from the measurement of the time constant of this transient as a function of temperature. The initial magnitude of the transient is related to the concentration of the traps. The form of this technique used in DLTS makes use of one or more voltage pulses applied to a sample in order to define the initial conditions.

For simplicity, this discussion will be focused on n-type material in an asymmetric p^+n diode. In more symmetric junctions, traps on both sides of the junction give comparable signals. However, for the highly asymmetric case the depletion region is primarily on the lightly-doped side of the junction. Thus, this discussion will consider only those traps in the lightly-doped n-side of the p^+n diode.

The capture and thermal emission rates for minority

carriers (holes in this case) are defined as C_1 and e_1 respectively. The capture and thermal emission rates for majority carriers (electrons) are defined as C_2 and e_2 respectively. In the quiescent state of the system, the diode is reverse biased and the observable traps are within the depletion region. Thus, the capture rates are zero and the occupation of the level is determined by the thermal emission rates e_1 and e_2. As a result, the steady-state electron occupation of a level is

$$\bar{n}_2 = \frac{e_2}{e_1+e_2} N_T \tag{5}$$

where N_T is the concentration of the trap. In this example a hole (minority-carrier) trap is defined as one which tends to be empty ($\bar{n}_2 = o$) of electrons and thus capable of capturing them. Likewise, an electron (majority-carrier) trap is one which tends to be full ($\bar{n}_2 = N_T$) of electrons and thus capable of having a trapped electron recombine with a hole. Therefore, in accordance with Eq. (5), a hole trap must have $e_1 >> e_2$ and an electron trap $e_2 >> e_1$. The emission rates are proportional to a Boltzmann factor, and thus, depend exponentially on the energy difference between the trap level and the conduction band edge (electron emission) or between the trap level and the valence band edge (hole emission). As a result, electron traps tend to be in the upper half of the gap and hole traps in the lower half.

A capacitance change is caused by using a bias pulse to introduce carriers, and thus change the electron occupation

of a trap from the steady state value in Eq. (5). As this population returns to equilibrium, the capacitance returns to its quiescent value. The transient is an exponential function of time with a rate constant to $e_1 + e_2$. One of these rates usually dominates; thus the transient rate for a majority-carrier trap is nearly e_2 and for a minority-carrier trap is nearly e_1. The sign of the capacitance change depends on whether the electron occupation of the trap has been increased or decreased by the pulse. An increase in trapped minority carriers causes an increase in the junction capacitance. The capacitance transient due to a minority-carrier trap is always positive and is induced only by injected minority carriers. However, the transient due to a majority-carrier trap is always negative and is induced only by the majority carriers.

An injection pulse momentarily drives the diode into forward bias and injects majority carriers into the depletion region. During such a pulse, the capture rates (C_1 and C_2) and the trap concentration (N_T) relate the steady-state electron occupation as

$$n_2 = \frac{C_2}{C_1+C_2} N_T \qquad (6)$$

The injection pulse introduces electrons such that $C_2 >> C_1$ and thus completely fills the trap with electrons.

The essential feature of the DLTS technique is the ability to set an emission rate window such that the measurement apparatus only responds when it sees a transient with a rate

within this window. Thus, if the emission rate of a trap is varied by varying the temperature, the instrument will show a response peak at the temperature where the trap emission rate is within this window. These emission rates are thermally activated and by the principle of detailed balance can be given as

$$e_R = \frac{\sigma \langle V \rangle N_D}{g} e^{(-E/KT)} \qquad (7)$$

where e_R is the thermal emission rate of a trapped electron, σ is the capture cross section, $\langle V \rangle$ is the mean thermal velocity of carrier, N_D is the effective density of states, g is the degeneracy of the trap level, E is the activation energy, K is Boltzmann's constant, and T is the peak temperature of the trap level.

Appendix B

Capacitance Time Constant and Energy Level Derivations

The capacitance time constant (τ) can be derived in terms of the gate settings (t_1 and t_2) from the boxcar apertures. The time constant reaches a maximum value at the maximum of $C(t_1)-C(t_2)$ (Capacitance differences) vs. T (temperature) for a particular trap.

The normalized DLTS signal for a test sample is defined as

$$S(T) = [C(t_1)-C(t_2)]/\Delta C(o) \tag{8}$$

where

$\Delta C(o)$ = capacitance change due to the pulse at t = o

and the exponental transient is

$$S(T) = [\exp(-t_1/\tau)]-[\exp(-t_2/\tau)] \tag{9}$$

but

$$\Delta t = t_2-t_1$$

then

$$S(T) = \exp(-t_1/\tau)-[1-\exp(-\Delta t/\tau)] \tag{10}$$

From Eq. (10) the relationship between τ and t_1 and t_2 is determined by differentiating S(T) with respect to τ and setting the result equal to zero. The desired expression is then

$$\tau = \frac{t_1-t_2}{\ln(t_1/t_2)} \tag{11}$$

and the emission rate is

$$e_R = \frac{\ln(t_1/t_2)}{t_1 - t_2} \tag{12}$$

The emission rate can also be written as cited in Eq. (7) in Appendix A. This equation can be rewritten as

$$e_R = e_o \, e^{(-E/KT)} \tag{13}$$

where

$$e_o = \frac{\sigma \langle V \rangle N_D}{g} \tag{14}$$

The energy level or activation energy of a trapping state can be derived from Eq. (13) using the different emission rates at two distinct peak temperatures. The expression relating these parameters is

$$\frac{e_{R1}}{e_{R2}} = \frac{e_o \, e^{(-E/KT_1)}}{e_o \, e^{(-E/KT_2)}} \tag{15}$$

or

$$\frac{e_{R1}}{e_{R2}} = e^{-\frac{E}{K}\left(\frac{1}{T_1} - \frac{1}{T_2}\right)} \tag{16}$$

By taking the natural logarithm of both sides of Eq. (16), the expression becomes

$$\ln\left(\frac{e_{R1}}{e_{R2}}\right) = -\frac{E}{K}\left(\frac{1}{T_1} - \frac{1}{T_2}\right) \tag{17}$$

By rearranging Eq. (17), the desired expression is then

$$E = -\frac{\ln(e_{R1}/e_{R2})\, K}{\left(\frac{1}{T_1} - \frac{1}{T_2}\right)} \tag{18}$$

Vita

Clarence Edward Mayo was born on 13 October 1948 in Washington, D.C., the son of Frank W. Mayo and Willie Mae (Sutton) Mayo. He graduated in 1967 from McKinley High School in Washington, D.C. In June of 1972, he graduated from Howard University in Washington, D.C., received a Bachelor of Science Degree in Electrical Engineering, and was commissioned through the ROTC program. Immediately after graduating, he worked as an assistant power engineer for the Potomac Electric Power Company in Washington, D.C. After serving in this capacity for six months, he was assigned to the Satellite Control Facility in Sunnyvale, California where he served as a Satellite Software Systems Manager. Upon completion of his assignment in Sunnyvale, he entered the AFIT Graduate Electrical Engineering program in August 1976. He is a recipient of The American Society for Testing and Materials' student award for the year 1977.

Permanent Address: 354-1 Rio Verde Pl.
Milpitas, California 95035

This thesis was typed by Mrs. Sharon Maruna.

UNCLASSIFIED

SECURITY CLASSIFICATION OF THIS PAGE *(When Data Entered)*

REPORT DOCUMENTATION PAGE		READ INSTRUCTIONS BEFORE COMPLETING FORM
1. REPORT NUMBER AFIT/GE/EE/78-4	2. GOVT ACCESSION NO.	3. RECIPIENT'S CATALOG NUMBER
4. TITLE *(and Subtitle)* DEEP LEVEL TRAP SPECTROSCOPY OF GALLIUM ARSENIDE		5. TYPE OF REPORT & PERIOD COVERED MS Thesis 6. PERFORMING ORG. REPORT NUMBER
7. AUTHOR(s) Clarence E. Mayo		8. CONTRACT OR GRANT NUMBER(s)
9. PERFORMING ORGANIZATION NAME AND ADDRESS Air Force Institute of Technology (AFIT-EN) Wright-Patterson AFB, Ohio 45433		10. PROGRAM ELEMENT, PROJECT, TASK AREA & WORK UNIT NUMBERS
11. CONTROLLING OFFICE NAME AND ADDRESS Air Force Avionics Laboratories (AFAL/DHR) Wright-Patterson AFB, Ohio 45433		12. REPORT DATE March 1978 13. NUMBER OF PAGES 78
14. MONITORING AGENCY NAME & ADDRESS *(if different from Controlling Office)*		15. SECURITY CLASS. *(of this report)* Unclassified 15a. DECLASSIFICATION/DOWNGRADING SCHEDULE

16. DISTRIBUTION STATEMENT *(of this Report)*

Approved for public release; distribution unlimited.

17. DISTRIBUTION STATEMENT *(of the abstract entered in Block 20, if different from Report)*

18. SUPPLEMENTARY NOTES

Approved for public release; IAW AFR 190-17

JERRAL F. GUESS, Captain, USAF
Director of Information

19. KEY WORDS *(Continue on reverse side if necessary and identify by block number)*

Capacitance transient
Trapping states
Epitaxial GaAs
Deep Levels
Electron Irradiation

20. ABSTRACT *(Continue on reverse side if necessary and identify by block number)*

Trapping states in epitaxial GaAs induced by 1 MeV electron irradiation were measured by transient capacitance. N-type epitaxial GaAs samples with "buffer" layer were irradiated at room temperature with 1 MeV electrons, at doses ranging from $10^{14}cm^{-2}$ to $10^{16}cm^{-2}$. Carrier removal, changes of concentration profile, diode behavior, and C-V characteristics were measured as a function of electron dose. Transient capacitance spectroscopy techniques were used to measure deep trapping

DD FORM 1 JAN 73 1473 EDITION OF 1 NOV 65 IS OBSOLETE

UNCLASSIFIED

SECURITY CLASSIFICATION OF THIS PAGE *(When Data Entered)*

Concentrations of trapping states as a function of electron dose were measured and related to the carrier concentration measurements. The usual electron-induced trapping states with significant variations were noted. Variations of spatial depth of the traps as a function of irradiation and thermal cycling were observed. Samples were in the form of FET test patterns for correlation of material properties and device performance.